Experimental results of transient testing at the amine plant at Technology Centre Mongstad: open-loop responses and performance of decentralized control structures for load changes

Corresponding author*: Rubén Mocholí Montañés

Address: Department of Energy and Process Engineering

NTNU – Norwegian University of Science and Technology

Kolbjørn Hejes vei 1b, Varmeteknisk * B347

NO – 7491 Trondheim, Norway

Phone: +47 735093722

e-mail address: ruben.m.montanes@ntnu.no

Experimental results of transient testing at the amine plant at Technology Centre Mongstad: open-loop responses and performance of decentralized control structures for load changes

Rubén M. Montañés *[a], Nina E. Flø [b], Lars O. Nord [a]

[a] Department of Energy and Process Engineering, NTNU - Norwegian University of Science and Technology, Kolbjørn Hejes v. 1B, 7491 Trondheim, Norway;

[b] Technology Centre Mongstad, 5954 Mongstad, Norway;

*Correspondence: ruben.m.montanes@ntnu.no; Tel.: +47-73593722

KEYWORDS: Post combustion; chemical absorption; MEA; CO_2 capture; dynamic behaviour; pilot plant; operational flexibility.

Abstract

Flexible operation of combined cycle thermal power plants with chemical absorption post combustion CO_2 capture is a key aspect for the development of the technology. Several studies have assessed the performance of decentralized control structures applied to the post combustion CO_2 capture process via dynamic process simulation, however there is a lack of published data from demonstration or pilot plants. In this work, experiments on transient testing were conducted at the amine plant at Technology Centre Mongstad, for flue gas from a combined cycle combined heat and power plant (3.7 to 4.1 CO_2 vol%). The experiments include six tests on open-loop responses and eight tests on transient performance of decentralized control structures for fast power plant load change scenarios.

The transient response of key process variables to changes in flue gas volumetric flow rate, solvent flow rate and reboiler duty were analyzed. In general the process stabilizes within 1h for 20% step changes in process inputs, being the absorber column absorption rates the slowest process variable to stabilize to changes in reboiler duty and solvent flow rate. Tests on fast load changes (10%/min) in flue gas flow rate representing realistic load changes in an upstream power plant showed that decentralized control structures could be employed in order to bring the process to desired off-design steady-state operating conditions within (<60 min). However, oscillations and instabilities in absorption and desorption rates driven by interactions of the capture rate and stripper temperature feedback control loops can occur when the rich solvent flow rate is changed significantly and fast as a control action to reject the flue gas volumetric flow rate disturbance and keeping liquid to gas ratio or capture rate constant.

1. Introduction

The anthropogenic greenhouse gas emissions have led to the increase in concentration of CO_2 in the atmosphere, being the main cause of global warming and climate change [1]. Carbon capture and storage (CCS) is a group of technologies that can significantly reduce the CO_2 emissions from the use of fossil fuels for thermal power generation and other industrial sources [2]. According to the International Energy Agency, the global average carbon intensity of the power sector in 2015 was around 500 $kgCO_2/MWh$ and global average of 100 $kgCO_2/MWh$ should be achieved by 2040 to be consistent with a 2 °C scenario [3]. In this regard, natural gas combined cycle power plants could be considered today as low carbon alternatives

due to their carbon intensity levels of 400-450 *kgCO_2/MWh*. However, in the mid-to-long term it might be required to decarbonize natural gas combined cycle power plants by retrofitting existing units with post-combustion CO_2 capture (PCC) or by designing new CCS power plants. Post-combustion CO_2 capture with chemical absorption using amines is considered a mature technology for CCS from thermal power plants [4], and it has been demonstrated at commercial scale in CCS projects from coal-fired thermal power plants, at Boundary Dam project in Canada [5] and the Petra Nova project in US [6].

In current and future energy systems with high penetration of renewable energy sources, the operational role of thermal power plants changes. Load-following operation of thermal power plants and flexible operation will become a key aspect of the technology development [7, 8]. Thermal power plants will need to cycle on and off and to ramp up and down more frequently, rapidly and cost-effectively [9], in order to keep the balance between generation and demand and back-up renewable energies, and to be competitive in the power markets. Regarding thermal power plants with CCS, load following capabilities and operational flexibility are considered as extremely important aspects of the technology [4, 10, 11].

The transient performance of the post-combustion CO_2 capture system during start-up and shut down, load changes and flexible operation strategies is a key aspect that has been subject of extensive study via dynamic process simulation tools. Dynamic process modeling and simulation has been used to assess aspects of flexible operation and control of thermal power plants integrated with PCC [12-18]. Bui et al. [19] concluded that work should focus on providing sets of transient data from PCC pilot plants for dynamic process model validation and for gathering more knowledge on pilot plant flexible operation. Nevertheless, pilot plant testing requires expensive resources and there are limited published data with transient operation available in the literature. Transient pilot plant testing is normally conducted with two methodologies, open-loop transient testing or testing flexible operation scenarios.

During open-loop testing, step changes are applied in set-points of some inputs to the plant, and the transient response of the process variables of the system are monitored. This approach helps to characterize and analyze the transient response of the process and contributes to generate suitable data sets that can be utilized for dynamic process model validation. The open-loop tests are desired since they minimize data variability and also allow to identify the effects that one input or disturbance to the plant have on important process variables of the process. In addition, the influence of the control loops of the advanced control layer of the chemical plant on the resulting transient performance is reduced. Test campaigns have been conducted for the chemical absorption process with aqueous monoethanolamine (MEA). Faber et al. [20] conducted transient tests with the Esbjerg pilot plant at the coal-fired power plant Esbjergværket, in Denmark. They conclude that the capture process acts as a buffer for any perturbation at the inlet, and that the process required between 1 h 15 min and 1 h 45 min for stabilization after the disturbances applied. Validation of dynamic process models with data from Esbjerg transient tests was conducted by Åkesson et al. [21] and Gaspar et al. [22]. Flø et al. conducted transient tests at the Gløshaugen pilot plant to provide sets of data and carry out dynamic process model validation by applying set-point step changes [23]. Several publications have described transient tests by applying step-changes in main inputs to the process in pilot plants with the purpose of generating data for dynamic process model validation [15, 24-27]. In addition, research is carried out to reduce the heat required for solvent regeneration [28, 29].

Bui et al. [27] conducted a flexible operation campaign at the AGL Loy Yang power station, with the post-combustion CO_2 capture pilot plant that treats a slipstream of flue gas from the coal fired power plant.

This experimental study verifies that flexible operation is feasible, and highlights the lack of experimental tests involving control structure analysis during dynamic operation of pilot plants. Tait et al. [30] conducted a pilot scale study of dynamic response scenarios for flexible operation of the PCC process. Five scenarios were tested: gas turbine shut down, gas turbine start-up and three scenarios for power output maximization. Their conclusions include that large solvent inventory increases total circulation times, and those have a significant effect on capture rate during dynamic operation, and that the plant requires longer time for stabilization when operated with larger amounts of solvent inventory.

A key aspect of transient operation of the process is related to the control structure implemented in the PCC plant. The transient response of the system to disturbances differs for different control strategies. Several contributions in the literature have utilized validated dynamic process models and simulations in order to assess the controllability and evaluated the capability of different control structures to reject disturbances [13, 14, 31-33]. The work conducted via dynamic process simulation contributes to develop the learning curve for flexible operation of the system in the scarcity of commercial scale operational experience. However, to the authors knowledge these control strategies have not been implemented or tested at pilot or demonstration scale plants. Therefore, this work focuses on getting hands on experience on the implementation of decentralized control structures and testing them for fast load change disturbances at a pilot plant for flue gas from a natural gas fueled combined cycle power plant. In this work the tests were conducted at the amine plant at Technology Centre Mongstad (TCM DA), which is a larger scale pilot plant than the pilot plants and laboratory set-ups employed for previous transient testing dedicated papers available in the literature [20, 27, 30].

The objectives of this work were to evaluate the performance of a demonstration plant to open-loop step-changes in main inputs to the process, and to evaluate the performance of decentralized control structures applied to a demonstration PCC plant. The tests were conducted at the amine plant at Technology Centre Mongstad (TCM DA) in Norway during the MEA-3 test campaign [34]. Validated dynamic process models developed in previous work [35] were employed to carry out the test planning. The tests were conducted at the plant for disturbances representing fast load changes of the upstream power plant.

2. Chemical absorption pilot plant with amines at Technology Centre Mongstad

The amine plant at the Technology Centre Mongstad is a flexible plant that can be configured to treat flue gas with a wide range of CO_2 concentrations and with different absorption solvents. That includes flue gas coming from the residue fluid catalytic cracker (RFCC) of the Statoil refinery placed next to TCM DA facility with typical CO_2 concentration of coal-fired power plants (14 vol% CO_2), and flue gas from the natural gas combined cycle combined heat and power plant (CHP) with a CO_2 concentration of around 3.5 vol%. Figure 1 shows a simplified process flow sheet of the plant when it is configured with the CHP stripper. Details on the amine pilot plant are presented in previous modeling, validation and simulation work by Montañés et al. [24, 35], and other published works with the amine plant when using aqueous MEA as chemical solvent [36-38]. The process configuration consists of the simple absorber-desorber solvent regeneration process with chemical absorption of CO_2, and the chemical solvent employed was 30% aqueous MEA. The plant can capture around 80 tonCO_2/day for operation with CHP gas conditions and the flue gas volumetric flow rate capacity is 60 000 Sm^3/hr. Here standard S means 1 atm and 15 °C.

A slipstream of flue gas coming from the natural gas fired CHP plant is conducted by a blower towards the pilot plant. The blower has variable speed drives that allows manipulating the flue gas volumetric flow rate to the plant. As shown in Figure 1, a closed-loop controller on *FT1* allows to specify the set-point of the flue gas volumetric flow rate at the inlet of the absorber, by manipulating the speed of the blower at the inlet of the direct contact cooler (DCC). The blower also provides the pressure required to overcome the pressure drop induced by the DCC and absorber column.

The flue gas is conducted towards the DCC, where it is cooled down and saturated with a countercurrent flow of water. The flue gas flows through the absorber column, were it contacts the chemical solvent in the absorption packing segments of the column. Then it flows towards the two water wash sections that are operated to control the water balance of the plant and to limit the gas emissions. A water make-up stream is injected in the water wash system. The packing material in which the chemical solvent meets the flue gas, and where the heat and mass transfer phenomena related to the exothermic chemical absorption process occurs, is divided in three sections. The three sections consist of structured stainless steel Koch Glitsch Flexipack 2X [38]. The packing has a rectangular cross section of 3.55 x 2 m^2 with a total of 24 m of absorber packing (12 m at the bottom, 6 m in the middle and 6 m at the top). The water wash section consists of two sections of 3 m each, of structured stainless steel Koch Glitsch Flexipack 2Y HC [38]. The depleted flue gas leaves the process at the top of the column.

The solvent loaded with CO_2 (rich solvent), accumulates in the absorber sump. The absorber sump at TCM DA amine plant also has the function of surge tank, in which the solvent will accumulate at different operating loads of the plant, and where the water streams of the process (from water wash and stripper reflux) are recirculated. The rich flow (*FT5*) is pumped by a variable speed pump, which sends the flow through the lean/rich integration heat exchanger, where the rich solvent is heated up by the lean solvent from the stripper bottom. The lean/rich heat exchanger consists of a plate and frame heat exchanger. The solvent loaded with CO_2 flows downwards through the stripper packing material, consisting of 8 m of Koch Glitsch Flexipack 2X [38] with diameter of 1.3 m, where it meets the stripping vapors of CO_2 and H_2O generated in the reboiler. The reboiler consists of a thermosiphon type heat exchanger, where heat is provided by steam from the refinery. Details on the steam supply system are presented in Faramarzi et al. [37]. The stripping vapors flow through a water wash section were some more water is removed, and then through the overhead cooler and condenser where the water condensates. The CO_2 rich stream, product CO_2 (*FT3*), is sent to the CO_2 stack. The lean solvent accumulates in the stripper sump, and it is pumped towards the lean/rich heat exchanger and the direct contact cooler by means of the lean solvent pump. The lean amine cooler allows to control the temperature of the lean solvent at the inlet of the absorber column, by manipulating the flow of cooling water.

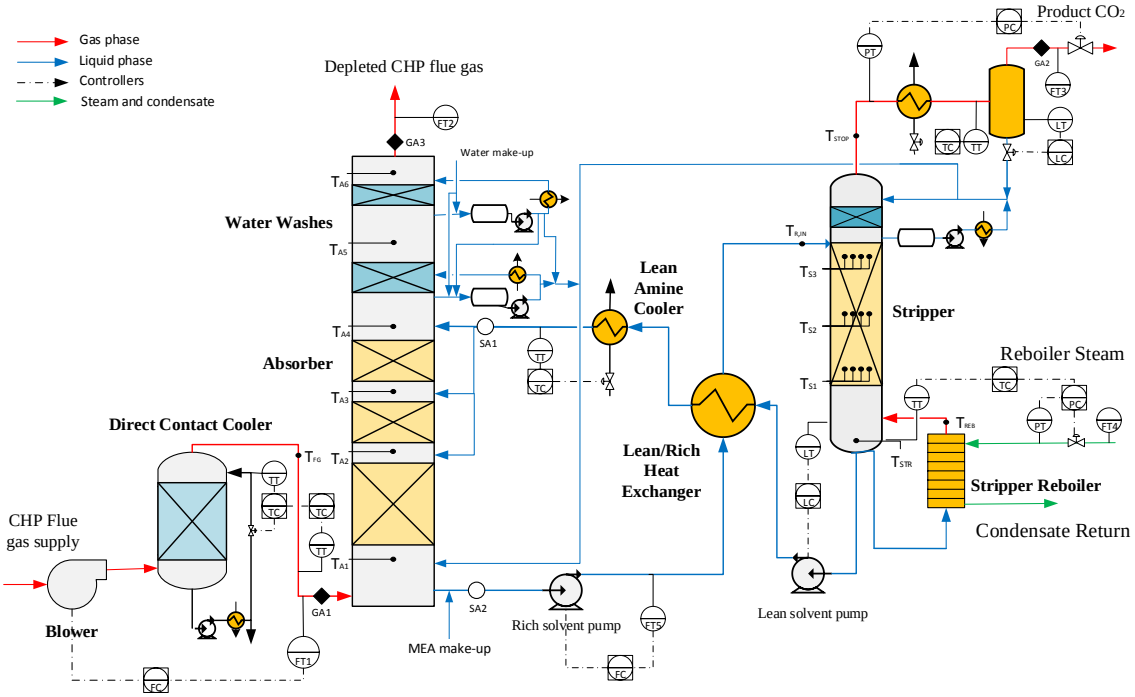

Figure 1 Simplified process flow sheet of the amine plant at TCM DA when configured to treat flue gas from the CHP plant. Figure obtained and modified from [35]. The figure shows transmitters (-T), Controllers (-C) and the location of gas analyzers (GA), solvent analysis sampling points (SA). Flow transmitters (FT), level transmitters (LT), temperature transmitters (TT), pressure transmitters (PT).

3. Description and objectives of experiments

3.1. Process conditions during the tests

The pilot plant was operated under similar process conditions as in the baseline presented in Faramarzi et al. [37]. This was implemented by setting similar independent parameters, i.e., the process variables that are available for control for the operators [39]. The initial steady-state process conditions for the control structures testing period for flue gas at the inlet of the absorber column (refer to GA1 in Figure 1) are presented in Table 1. Note that the steady-state process conditions presented in this section of the paper were obtained as averaged values during 25 min of steady-state operation before test 1 on control structures was initiated (refer to Figure 2 and section 3.2). This differs from the baseline data from [37], which have been obtained with a larger amount of operating hours and with third party verification of instrumentation and data.

During the whole test period of open-loop testing (refer to section 3.1) and part of the test period for control structure testing, flue gas at the inlet of the absorber had a higher CO_2 content of around 4.1 vol% compared to typical values of CO_2 content of around 3.7 vol% when running the plant with CHP flue gas. This was because the CHP power plant located upstream the pilot plant process was fired with a different fuel during parts of the test period, the fuel consisting of a mixture of natural gas and refinery gas. From a pilot plant operation perspective, this can be considered as a boundary condition and could not be modified. That resulted in a lower capture rate (around 74% instead of around 85% [37]) and higher specific reboiler

duty (*SRD*), 3.80 kJ/kgCO_2 instead of 3.63 kJ/kgCO_2 [37] compared to the baseline presented in [37]. During the test period for tests 1 to 8, the CO_2 vol% changed; refer to Figure 2. The CO_2 content in flue gas was around 4.1 vol% until around 29 hours of testing in which it was reduced in a close-to-step manner towards 3.7 vol%. This corresponded to a disturbance during the test 6 (refer to section 3.3.2). In addition, the CO_2 content was reduced to around 3.6 vol% at around 32.5 hours of testing. This happened during test 7. The effect of these disturbances is discussed in section 4.2.2. The flue gas supply temperature can be controlled by manipulating the cooling water temperature at the inlet of water stream to the DCC; refer to Figure 1. For the experiments, the flue gas temperature was controlled to around 30 °C. Note that, during open-loop testing, the CO_2 vol% was close to 4.1 for all the tests A to F; refer to section 3.1.

Process conditions of aqueous MEA solvent during the initial steady-state conditions of test 1 on control structure testing, are presented in Table 2. Solvent lab samples were collected regularly during the testing at the inlet of the absorber and at the outlet of absorber (refer to SA1 and SA2 in Figure 1). During the tests, lean MEA concentration was slightly below 30 wt% MEA. Note that consistent inventory control and a proper configuration of the regulatory control layer of the plant is required for stable operation of the process [40]. The solvent flow network is defined by changing the set-point of the rich solvent mass flow rate, which acts as a throughput manipulator (TPM) of the process. The lean solvent flow rate is manipulated with a PI controller to control the stripper's sump level, so it is automatically adjusted when changing the rich solvent flow rate, while the temperature of the lean solvent at the inlet of the absorber column is controlled at a value of around 37 °C by a varying stream of cooling water to the amine cooler. Table 3 shows the solvent inventories at different operating conditions of the plant. Figure 3 shows the block diagram with the different main volumes of equipment at the pilot plant, and the circulation times at each of these components. The circulation times are calculated considering rich and lean volumetric flows and solvent inventories at the different components of the pilot plant for three selected operating conditions. Figure 3 shows the influence of solvent flow rate on the circulation times. At high solvent flow rates (case 1 in Table 3), the resulting circulation times were smaller, with a total circulation time of the pilot plant of around 41 minutes, while for the case with lowest solvent flow rate (case 3 in Table 3) the total circulation time was around 71 minutes. This has implications on the transient operation of the plant, since when the process is operated with lower solvent flow rates, it requires longer times to reach steady-state operating conditions, according to dynamic process simulation analyses [35]. When the solvent circulation flow rate is decreased, excess solvent accumulates mainly in the absorber sump, i.e. the absorber sump also has the function of a surge tank. This can explain the increase in solvent hold up in the absorber sump from Case 1 to Case 3 (see Table 3). Together with the lower solvent flow rate, it results in an increase in circulation time from around 3 minutes to around 10 minutes in the absorber sump; refer to Figure 3. Note that during the tests presented in this work, the pilot plant was operated with a relatively low amount of solvent inventory in the absorber sump, 3.7 m^3 to 5.7 m^3,compared with other test campaigns (Montañés et al. reported a total solvent inventory in the absorber sump of 8.1 m^3 [35]).

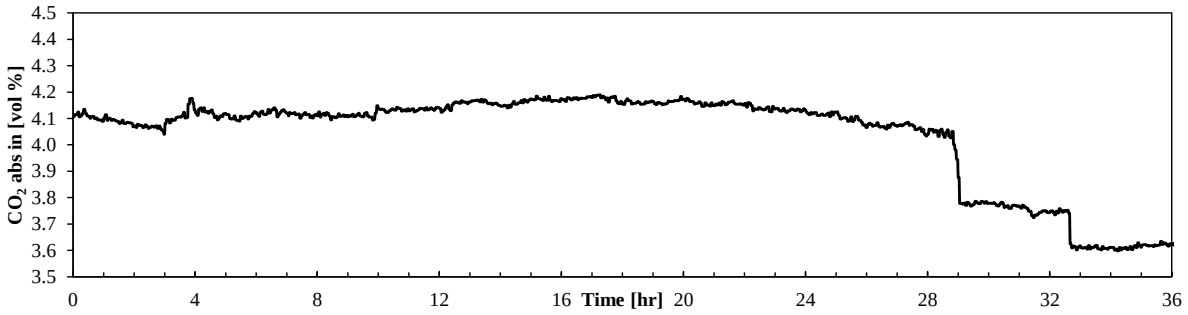

Figure 2. CO_2 content of flue gas at the absorber inlet during the hours of testing for control structures (test 1 to 8). CO_2 vol% (wet) measured with the gas chromatograph (GC) installed at TCM DA at point GA1 (refer to Figure 1).

Table 1. Flue gas averaged process conditions at the inlet of the absorber column, refer to GA1 in Figure 1. The process conditions are the averaged values during 25 min of operation before the first test 1 started, refer to section 3.3.1.

CHP flue gas process conditions	Unit	Value
Operating capacity	%	100
CHP flue gas supply rate F_{gas}	Sm^3/hr	60 528
CHP flue gas supply temperature	°C	30.0
CPH flue gas supply pressure	barg	0.0485
CHP flue gas supply CO_2 (wet)	vol%	4.12
CHP flue gas supply O_2 (wet)	vol%	14.09
CHP flue gas supply water content	vol%	4.43
Depleted flue gas temperature	°C	31.1

Table 2. Solvent averaged process conditions at different locations of the plant, refer to Figure 1. The process conditions are the averaged values during 25 min of operation before the first test 1 started, refer to section 3.3.1. Lean loading L_l and lean MEA concentration c_{MEA} are taken at the *SA1* sampling point, while rich loading at *SA2* sampling point.

Solvent process conditions	Unit	Value
Lean MEA concentration	wt%	28.7
Lean CO_2 loading	mol CO_2/mol MEA	0.22
Lean amine supply flow rate	kg/hr	62 283
Lean amine supply temperature	°C	36.8
Lean amine density	kg/m^3	1069
Rich CO_2 loading	mol CO_2/mol MEA	0.53
Rich solution supply flow rate	kg/hr	65 663
Rich solution supply temperature	°C	111.1
Rich solution density	kg/m^3	1 120
Rich solution return temperature	°C	32.8
Lean solution return temperature	°C	120.4

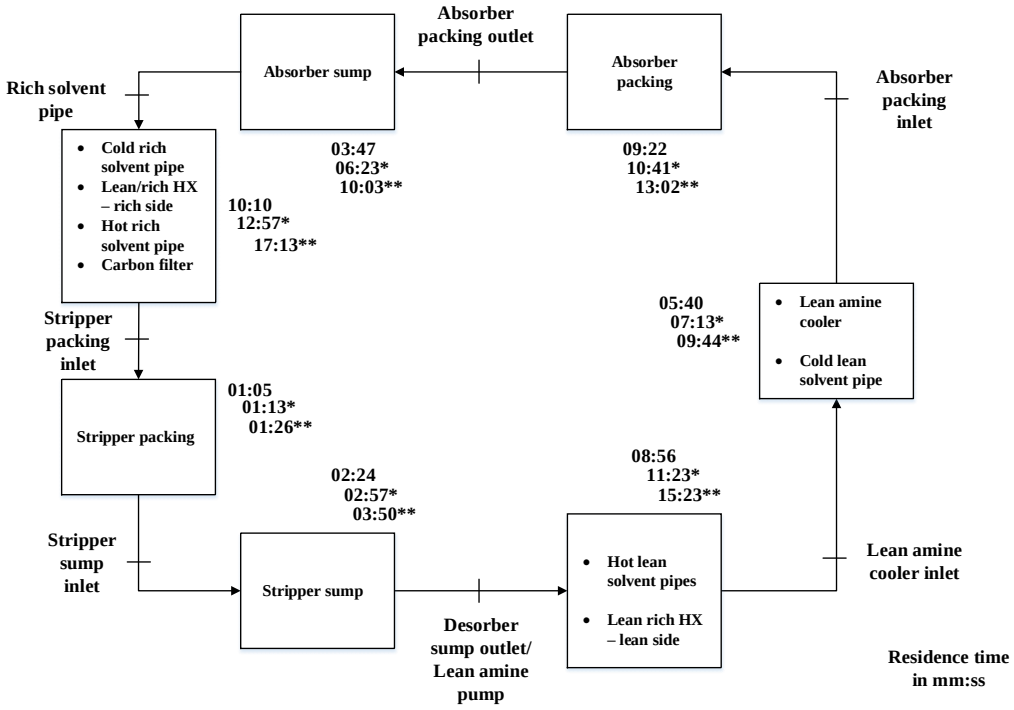

228

229 **Figure 3. Block diagram of solvent inventory distribution at the amine plant of Technology Centre Mongstad when operated**
230 **with CHP flue gas configuration. Circulation times are shown for the plant operated with rich solvent flow rate (F_{solv}) of 65**
231 **700 kg/hr (Case 1 on 17 July 2017 at 11:30), 52 000 kg/hr (*) (Case 2 on July 23 at 04:00) and 40 000 kg/hr (**) (Case 3 on**
232 **17 July at 23:00). The circulation times are calculated considering solvent inventory distribution in Table 3. The circulation**
233 **time in each unit of the process is expressed in mm:ss.**

234 **Table 3. Solvent inventory distribution at different components of the amine pilot plant at TCM DA during the tests**
235 **campaign. The three cases were selected to represent different process conditions with different rich solvent mass flow rate**
236 **(F_{solv}) of 65 700 kg/hr (Case 1 on 17 July 2017 at 11:30), 52 000 kg/hr (Case 2 on July 23 at 04:00) and 40 000 kg/hr (Case 3**
237 **on 17 July at 23:00). Total circulation times are calculated considering the addition of circulation times in Figure 3, for each**
238 **case.**

Solvent flow rates	**Case 1**	**Case 2**	**Case 3**
Rich solvent mass flow rate [kg/h]	65 630	52 025	40 042
Rich solvent volumetric flow rate [m^3/hr]	58.7	46.4	35.7
Lean solvent mass flow rate [kg/hr]	62 286	49 074	37 487
Lean solvent volumetric flow rate [m^3/hr]	58.0	45.8	33.9
Pilot plant component	**Solvent inventory Case 1 [m^3]**	**Solvent inventory Case 2 [m^3]**	**Solvent inventory Case 3 [m^3]**
Absorber sump	3.67	4.87	5.67
Absorber packing	9.09	8.15	7.36
CHP stripper packing	1.07	0.94	0.85
CHP stripper sump	2.35	2.28	2.29
CHP reboiler	0.42	0.42	0.42
Carbon filter	6.1	6.1	6.1
Aold rich solvent pipe	2.22	2.22	2.22
Aold lean solvent pipes	5.21	5.21	5.21
Hot rich solvent pipe	1.13	1.13	1.13

Hot lean solvent pipes (including reboiler pipes)	8.2	8.2	8.2
Lean/rich hx - lean side	0.485	0.485	0.485
Lean/rich hx - rich side	0.485	0.485	0.485
Lean amine cooler	0.29	0.29	0.29
TOTAL inventory	40.7	40.7	40.8
Total circulation time [min]	41.4	54.6	71.4

The process operating conditions at the desorber-reboiler section of the process during test 1 on control structures are presented in Table 4. The steam flow rate is changed at the plant by manipulating the set-point of the steam pressure, which can be as well set on stripper sump temperature control; refer to section 3.3. The stripper overhead pressure is controlled by the product CO_2 valve to a set-point of around 1.9 bar. The actual reboiler duty is calculated considering the steam and condensate process conditions (pressures, temperatures and mass flow rate) as presented in literature [35, 39].

Table 4. Process conditions at the desorber and reboiler sections of the TCM DA amine plant during initial steady-state operating conditions of test 1 (refer to section 3.3.1).

Desorber process conditions	Unit	Value
Reboiler steam flow rate	kg/hr	6 012
Reboiler steam temperature	°C	164.6
Reboiler steam pressure	barg	2.90
Stripper overhead pressure	barg	0.90
Stripper overhead temperature	°C	98.5
Reboiler solution temperature	°C	124.0
Reboiler duty	kW	3 737
Specific reboiler duty	GJ/ton CO_2	3.80
Product CO_2 flow rate	kg/hr	3 593
Product CO_2 discharge temperature	°C	12.9
Product CO_2 water content	vol%	0.98

3.2. Tests on open-loop performance

The purpose of the open-loop dynamic tests was to investigate the transient performance of the PCC pilot plant by implementing open-loop step-changes. The analysis aims to assess transient response of the plant to multiple and non-simultaneous step-changes in key inputs/disturbances to the plant, namely (i) flue gas flow rate, and (ii) solvent flow rate. This was done for different flue gas capacities of the PCC plant, corresponding to different loads of the power plant. In addition, the data generated can be utilized for dynamic process model validation. The objectives were to:

- Investigate the transient response of the plant when reducing flue gas flow rate (step-change) and when increasing flue gas flow rate (step-change).
- Investigate the transient performance of the plant for changes in solvent flow rate, at different plant flue gas flow rate capacities (different loads of the plant).

The tests were conducted at TCM DA during a total of 48 hours of testing. Table 5 shows the main inputs to the plant during the tests, in terms of steam flow rate (F_{steam}), rich solvent flow rate (F_{solv}) and flue gas flow rate (F_{gas}). A step-change is applied and then enough time (8 hours) is allowed for the process to stabilize, when the next step is applied.

Table 5. Test matrix for open-loop tests during the MEA3 test campaign. The values for the main inputs to the process are shown: flue gas volumetric flow rate (F_{gas}), rich solvent flow rate (F_{solv}), steam flow rate (F_{steam}). The cell highlighted in grey color shows the main change from the previous test. The tests begun at 13:00 on 21 July 2017 and finalized on 23 July 2017 at 13:00.

Test	F_{gas} [Sm^3/hr]	F_{solv} [kg/hr]	F_{steam} [kg/hr]
Initial conditions	60 000	65 700	5 400
A (0 to 8 hr)	47 000	65 700	5 400
B (8 to 16 hr)	47 000	52 000	5 100 (Oscillations)
C (16 to 24 hr)	47 000	65 700	5 400
D (24 to 32 hr)	60 000	65 700	5 400
E (32 to 40 hr)	60 000	52 000	5 100
F (40 to 48 hr)	60 000	65 700	5 400

3.3. Tests on decentralized control structures

The objective of the tests on decentralized control structures was to get experience with the operation and control of the process during transient events of fast load changes, and to observe the capability of the system to reject disturbances in terms of fast load changes of the upstream power plant. Two decentralized control structures were implemented, considering as main degrees of freedom for operation (manipulable variables), the rich solvent mass flow rate (F_{solv}) and the steam flow rate to the reboiler (F_{steam}).

For significant load changes in a combined gas and steam turbine cycle power plant, the load change is driven by gas turbine (GT) load reduction or increase. The gas turbine load is changed, and this normally implies a significant change of the exhaust mass flow rate sent to the heat recovery steam generator. Then, the steam cycle is automatized to follow this change in load and steam production and reach the new steady-state operating conditions [14, 41]. When the power plant is integrated with CCS, the load change represents a disturbance to the PCC unit in terms of flue gas mass flow rate, composition and temperature, and the available steam from the power plant. Two key aspects are required to define a load change in a combined cycle power plant, one is the minimum operating GT load of the system, and the other is the rate of change of load, the so called ramp rate.

The flue gas flow rate at minimum operating load and at different loads of the integrated system will depend on the GT technology and specific GT burner with controls, and the resulting exhaust gas characteristics. Simulation work by Jordal et al. [42] have reported that for a three-pressure reheat (3PRH)

configuration with PCC, the flue gas flow rate at minimum load of 40% GT load with a GE 9371FB GT (47.3 % combined cycle load with PCC), the flue gas flow rate is 64.5 % of the total flow rate at design point of 100% GT load. Rezazadeh et al. [43] sets the limit to 60% on minimum GT load for the integrated 3PRH combined cycle with PCC. The reasons are that at lower loads, the impacts on cost of electricity of the fuel price are more pronounced and that the stable and efficient operation of the main compressors of the system require a minimum flow of 70-75% of flue gas flow rate. In their study, 60% GT load for the General Electric 7 Frame (GE 7F.05) (69.4% combined cycle load with PCC) corresponds to 75.2 % flue gas flow rate with respect to the design point at 100% GT load [43]. Off-design simulations with the models presented by Montañés et al. [14] show that at 60% GT load with the Mitsubishi 701 JAC (66.48 % combined cycle with PCC load), the flue gas flow rate is 73.6% of design load. At 40% GT load, the flue gas mass flow rate is 61.9% of design load. In order to cover the full operating window presented in literature, it was decided in this work to define the minimum load of the PCC unit as 60% of flue gas volumetric flow rate (F_{gas}) in the absorber column (36 000 Sm^3/hr).

The ramp rate is the rate at which a power generator can change load. In general, faster ramp rates are the objectives of thermal power plant operators. A power unit that can ramp fast will be capable of following the variability in electricity prices in liberalized power markets, and save fuel costs [44]. However, excessively aggressive ramp rates will incur in lifetime reduction of components of the plant due to related thermal stresses [45, 46]. Load change ramp rates for natural gas combined cycle power plants are around 2-10%/min [46, 47]. In this work, it was decided to change the flue gas volumetric flow rate fed to the absorber column at TCM DA with a ramp rate of 10%/min. This can be considered a fast ramp rate for a combined cycle, since that would correspond to 13-14 %/min combined cycle load change or around 15-16 %/min GT load change, considering the steady-state off-design simulation results in Jordal et al. [42].

3.3.1. Tests with control structure with *L/G* control

The test matrix for tests 1 to 4 is presented in Table 6. For the four tests, rich solvent flow rate (F_{solv}) is manipulated manually to keep the liquid to gas ratio L/G in the absorber column to a value of around 1.04 kg/Sm^3. This was implemented at the pilot plant by changing the set-point of the rich pump flow rate controller (FT5 in Figure 1). The set-point of F_{solv} was changed with the same rate as the flue gas volumetric flow rate (F_{gas}) was changed. For a given test, the new set-point was defined to obtain a similar L/G ratio under initial and final steady-state operating conditions of the PCC pilot plant. In addition, steam flow rate is manipulated via a feedback control loop to control the stripper bottom liquid temperature (T_{str}), measured at the desorber sump.

Tests 1 and 3 represent a load decrease of the power plant resulting in flue gas volumetric flow changes from 100% to 80% and from 100% to 60%, respectively. The same rate of change was applied for solvent flow rate (F_{solv}) set-point. The objective was to test the influence of the magnitude of the disturbance on the capability of the control structure to reject the disturbance. Tests 2 and 4 represent load increase from the power plant, implemented by increasing the flue gas volumetric flow rate from 80% to 100% (test 2) and from 60% to 100% (test 4). In the four tests presented in Table 6, the flue gas volumetric flow rate was changed with a ramp rate of 10%/min.

Table 6. Test matrix for test 1 to 4 on load changes to test the performance of L/G ratio controller for fast cycling capabilities. Feed forwards (FF).

Test	Description	Active Controllers	Manual changes
1	Load reduction with L/G FF control	T_{str} at 120.9 °C	F_{gas} from 100% to 80% with ramp rate of 10%/min.
			F_{rich} from 65 000 to 52 000 kg/hr with set-point change in 120 sec, and resulting rise time of 5.5 min.
2	Load increase with L/G FF control	T_{str} at 120.9 °C	F_{gas} from 80% to 100% with ramp rate of 10%/min.
			F_{rich} from 52 000 to 65 000 kg/hr with set-point change in 120 sec, and resulting rise time of 3.5 min.
3	Load reduction with L/G FF control	T_{str} at 120.9 °C	F_{gas} from 100% to 60% with ramp rate of 10%/min.
			F_{rich} from 65000 to 40 000 kg/hr with set-point change in 120 sec, and resulting rise time of 5.5 min.
4	Load increase with L/G FF control	T_{str} at 120.9 °C	F_{gas} from 60% to 100% with ramp rate of 10%/min.
			F_{rich} from 40 000 to 65 000 kg/hr with set-point change in 120 sec, and resulting rise time of 5 min.

3.3.2. Tests with control structure with CO_2 capture rate control

Tests 5 to 8 were designed to test control structures with CO_2 capture rate being controlled. Controlling CO_2 capture rate has been found to be a suitable controlled variable to bring the process close to optimal operating conditions under the presence of disturbances [48]. Among the different methods to calculate capture rate at the amine plant at TCM DA presented by Faramarzi et al. [37], method 1 was selected. In method 1, CO_2 capture rate is calculated based on CO_2 product flow rate (F_{prod}) (refer to *FT3* in Figure 1) and the CO_2 supply at the inlet of the absorber column. The CO_2 capture (Cap_A) is defined in Equation (1), where $\dot{m}_{gas}$ is the mass flow rate of flue gas at the inlet of the absorber column and x_{CO_2} is the mass fraction of CO_2 in the flue gas at the inlet of absorber column. In addition, CO_2 capture rate has been defined considering gas measurements in the absorber column (Cap_B), refer to method 3 in Faramarzi et al. [37] for details on instrumentation and calculation. It is calculated considering the CO_2 absorbed in the absorber column, as expressed in Equation (2), where $\dot{m}_{dep}$ is the mass flow rate of depleted flue gas and $x_{CO_2,out}$ is the mass fraction of CO_2 in the gas leaving the absorber. Note that Cap_A was utilized as controlled variable during tests 5 to 8, while Cap_B was used for observation and comparison only during all tests on control structures.

$$Cap_A = \frac{CO_2\ (Desorbed)}{CO_2(Supply)} = \frac{CO_2\ (Product)}{CO_2(Supply)} = \frac{F_{Prod}}{\dot{m}_{gas} \cdot x_{CO_2}} \quad (1)$$

$$Cap_B = \frac{CO_2\ (absorbed)}{CO_2(Supply)} = \frac{CO_2\ (supply) - CO_2(depleted)}{CO_2(Supply)} = \frac{\dot{m}_{gas} \cdot x_{CO_2} - \dot{m}_{dep} \cdot x_{CO_2,out}}{\dot{m}_{gas} \cdot x_{CO_2}} \quad (2)$$

For tests 5 to 8 Cap_A was controlled by manipulating the set-point of the rich mass flow rate (F_{solv}) cascade controller (refer to *FT5* in Figure 1). During the MEA3 campaign there was no time for fine tuning this controller. Therefore, a validated dynamic process model of the process was utilized for preliminary tuning of the controller [35]. The simple internal model control (SIMC) tuning rules [49] were employed to tune the master controller. For this cascade controller, the slave controller manipulates the pump speed to control the rich solvent mass flow rate, while the master controller manipulates the set point of the rich solvent flow rate controller to control Cap_A.

Firstly, open-loop testing responses to set-point change in solvent flow rate at the pilot plant were analyzed, and a closed-loop time constant of 3-5 min in the actual response of measured solvent flow (F_{solv}) to the set-point changes was observed. This is the closed-loop time constant of the slave controller in this cascade (inner). Normally, it is desired to have a good time scale separation in terms of closed-loop time constant between slave and master, a rule of thumb is a larger value by a factor of at least 5 [50]. Therefore, it was decided to start with a value of τ_c of 25 min. Simulations were conducted with the validated dynamic process models to tune the master controller with SIMC rules. The resulting values are a proportional gain *Kc* of 0.14 and an integral time K_I of 8 min. These are considered conservative for the controller tuning.

The test matrix for tests 5 to 8 is shown in Table 7. The tests consisted of volumetric flue gas flow rate (F_{gas}) decrease from 100% to 80% (tests 5 and 7) and increase from 80% to 100% (tests 6 and 8). For tests 5 and 6 the stripper bottom temperature (T_{str}) controller was also active. For tests 7 and 8, the steam sent to the reboiler was changed with a ramp set-point change. Cap_A was controlled by manipulating rich solvent mass flow rate in all tests with the closed feedback control loop.

Table 7. Test matrix for test 5 to 8 on load changes to test the performance of Cap_A ratio controller for fast cycling capabilities.

Test	Description	Active Controllers	Manual changes
5	Load reduction with Cap_A control	T_{str} at 120.9 °C	F_{gas} from 100% to 80% with ramp rate of 10%/min.
		Cap_A at 74%	
6	Load increase with Cap_A control	T_{str} at 120.9 °C	F_{gas} from 80% to 100% with ramp rate of 10%/min.
		Cap_A at 74%	
7	Load reduction with Cap_A control	Cap_A at 74%	F_{gas} from 100% to 80% with ramp rate of 10%/min.
			F_{steam} from 5 330 to 3 900 kg/hr in 40 min.
8	Load increase with Cap_A control	Cap_A at *74%*	F_{gas} from 80% to 100% with ramp rate of 10%/min.
			F_{steam} from 3 900 to 5 330 kg/hr in 40 min.

4. Results

4.1. Open-loop step responses

The results from open-loop testing experiments described in section 2.2 and Table 5 are shown and discussed in this section. In the figures shown the tests are separated by vertical lines, with a period of 8 h between experiments. The vertical lines indicate the time at which a step-change in a set-point is applied for a given test. Figure 4 shows the main inputs to the process for the six open-loop tests applied to the process, from A to F in Table 5. The inputs shown are flue gas volumetric flow rate (F_{gas}), solvent mass flow rate (F_{solv}), steam mass flow rate (F_{steam}) and the calculated actual reboiler duty ($\dot{Q}_{reb}$). Figure 5 shows the transient response for tests A to F of capture rates Cap_A and Cap_B, refer to equations (1) and (2) respectively, and CO_2 absorbed and CO_2 desorbed. Note that for tests C and F, a spike in Cap_B is observed at around 05:50, due to a failure in the measurement of CO_2 vol% in the depleted flue gas. Figure 6 shows the transient response of various temperatures in the absorber column, while Figure 7 shows the response of various temperatures in the desorber column and the reboiler. Figure 8 shows the response of lean and rich amine density at measured at locations SA1 and SA2 in Figure 1, and the lean and rich loading from lab samples taken during the open-loop tests.

In test A, flue gas flow rate set-point was reduced from around 60 000 Sm^3/hr to around 47 000 Sm^3/hr, while the rest of plant inputs were kept approximately constant; refer to Figure 4. This corresponds with a flue gas capacity of 100% to around 78%. The rise time on flue gas flow volumetric flow rate was around 16 min. So even if the set-point is changed in a step manner, it results in a second order response of measured flue gas volumetric flow rate, due to the integral action of the *PI* cascade controller; refer to FT1 in Figure 1. When reducing flue gas flow rate, the L/G ratio in the absorber column increased (from 1.04 kg/Sm^3 to 1.33 kg/Sm^3). This increased the capture rate of the process from around 68% to 86%; refer to test A in Figure 5. However, the CO_2 input into the plant was also reduced from around 4 670 kg/hr to around 3 600 kg/hr (not shown) as a result of decreasing flue gas flow rate. The combination of reduced CO_2 mass flow rate fed into the process with increased L/G ratio in the absorber column lead to similar absorption rate in the absorber column and desorption rate in stripper columns during initial and final steady-state conditions. In addition, the capture rate defined with the product flow rate Cap_A was more sensitive to changes in flue gas flow rate than the capture rate defined with the absorbed CO_2 or Cap_B. Cap_A peaked at around 13:25 with a value of 0.93 while Cap_B peaked at a value of around 0.88 at 13:32. This was because the stripper conditions were not significantly affected by the change in flue gas flow rate. The reduction in flue gas flow rate resulted in a shift in temperature profile in the absorber column, which resulted in higher temperature values; refer to temperatures T_{a1}, T_{a2} and T_{a3} in Figure 6 during test A. This is because a similar amount of CO_2 being absorbed leads to a similar amount of exothermal absorption heat being released, which is transferred to a lower volumetric flow of gas within the absorber column. The rise time of the transient response of T_{a3} was around 33 minutes, which was 17 minutes larger than the rise time on flue gas volumetric flow change of 16 minutes. This shows the effects of thermal and chemical inertia of the process to reach the new steady-state conditions of the temperature profiles in the absorber column when the flue gas flow rate is changed. The stripper temperature remained with similar values at initial and final steady-state conditions; refer to Figure 7. This suggests that a significant change in flue gas flow rate does affect the absorber temperature profiles while the stripper temperature profiles are not so sensitive to changes in flue gas flow rate, when the rest of process inputs are kept constant. The lean and rich amine density is kept

fairly constant as well during test A (refer to Figure 8) which is an indicator that there were not significant variations in CO_2 loadings for the change in flue gas flow rate. Considering the transient trajectories of Cap_A and Cap_B and 10% settling time, the process stabilized after approximately 45 min.

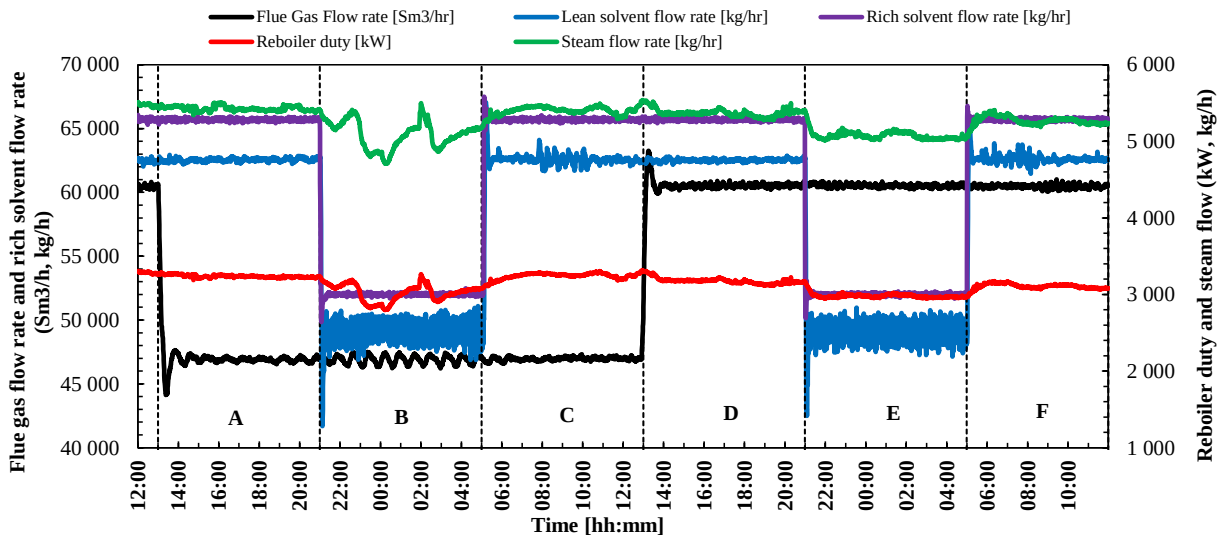

Figure 4. Open-loop tests during the MEA3 campaign. The test duration was 48 hours and was conducted between 12:00 on July 21 to 12:00 on July 23. The vertical lines indicate the time at which the set-point in flue gas flow rate (F_{gas}) or solvent flow rate (F_{solv}) was changed, and indicates the beginning of the tests from A to F; refer to Table 5. The steam flow rate (F_{steam}) and calculated actual reboiler duty ($\dot{Q}_{reb}$) are also shown.

Test B was designed to obtain the response of the process to a reduction of rich solvent flow rate set-point. For tests B and E in which rich solvent flow rate was reduced, there were oscillations of the measured lean solvent flow rate around the final steady-state point; refer to Figure 4. This is related to flashing in the lean/rich heat exchanger that leads to oscillations in solvent flow at the inlet of the stripper. In section 4.2, it is explained how this effect was solved for the closed-loop tests. In test B, the rich solvent mass flow rate (F_{solv}) set-point was changed from 65 700 kg/hr to 52 000 kg/hr at the beginning of test B, which corresponds with a 20% reduction of solvent flow rate. The fall time on measured F_{solv} is around 4 min, while for the lean solvent flow rate is around 6 min (despite of the oscillation found due to flashing). This shows that the solvent flow rate network responds generally faster than the rest of the process variables, and that changes in rich solvent flow rate are followed tightly by the lean solvent flow rate. However, from a control perspective, it would be desired to have an even faster response of measured rich solvent flow rate to changes in rich solvent flow rate set-point, for tighter control of process variables under load changes of the process. In addition, during test B some changes in steam flow rate were implemented (refer to Figure 4), which resulted in changes in reboiler duty during the test period. However, these unintended disturbances in reboiler duty applied to the process allowed us to add a discussion on the effects of changes in reboiler duty on the response of the system process variables. Figure 5 shows the response of CO_2 capture rates to the input changes in test B. It can be observed that CO_2 capture rates and CO_2 absorption and desorption rates were very sensitive to changes in reboiler duty. CO_2 desorption rate trajectory (and Cap_A) followed tightly the input trajectory in steam flow rate during test B, and CO_2 absorption (and Cap_B) followed with a larger delay. For example, steam flow rate (F_{steam}) peaked at time 02:01 during test B, while CO_2 desorption peaked 5 min later at 02:06 and CO_2 absorption peaked after 22 minutes at 02:23. This

shows two effects. One is that the performance of process variables in the stripper column respond fast to changes in reboiler duty, as it is also shown by the peak in T_{s3} at 2:04, i.e. 3 minutes later than steam flow rate; refer to Figure 7. The other is the effect of the circulation times through the recycle loop of chemical solvent on the response of the absorber column to changes in reboiler duty. The response of CO_2 absorbed (and Cap_B) shows a peak with a delay of around 22 minutes, with respect to the steam flow rate (F_{steam}) in the reboiler. As was shown in Figure 3 and Table 3 case 2, the solvent circulation time from stripper sump to absorber inlet is around 18.5 min, similar to the delay in CO_2 absorbed with respect to F_{steam}. When increasing steam flow rate the lean loading of the chemical solvent will be reduced. This increases the capacity of the solvent to absorb CO_2, and the driving force for CO_2 absorption at the top of the absorption column. However, the solvent has to circulate through the recycle loop, and the resulting circulation time from stripper sump outlet to absorber column inlet results in a delay in the CO_2 absorbed and Cap_B, and also on the absorber column temperature profiles; refer to Figure 6. In addition, it can be seen that Cap_A is more sensitive to changes in reboiler duty (peak at a value of 0.866) than Cap_B (peak at a value of 0.827). The reduction lean amine density observed in Figure 8 are good indicator of the fluctuations in lean loading above described, following the fluctuations in steam mass flow rate and resulting reboiler duty during test B.

Test C shows the response of the process to changes in rich solvent flow rate (F_{solv}) from 52 000 kg/hr to 65 700 kg/hr. In this case the rest of process inputs (flue gas flow rate and steam flow rate) were kept reasonably constant during the test. In this case the rise time for F_{solv} was 2 min while for lean solvent flow rate was around 6 min. An inverse response was observed in CO_2 absorbed Cap_B trajectory to change in F_{solv}. When lean solvent flow rate was increased, this resulted in an increase of the L/G ratio in the absorber column, in this case from 1.043 kg/Sm^3 to 1.325 kg/Sm^3. Initially, this resulted in an increase of the absorption rate of CO_2 in the absorber column, as can be seen in the trajectory of Cap_B and CO_2 absorbed in Figure 5. However, after a while the CO_2 absorbed decreased. The peak of CO_2 absorbed was reached at around 05:22 in test C, around 22 minutes after the set-point change in solvent flow rate was implemented. The change in the trend can be explained by that when solvent flow rate is increased (while keeping constant reboiler duty), the lean loading tends to increase. This was also observed by the decrease in reboiler solvent temperature which is considered a good indicator of solvent lean loading; refer to Figure 7. However, this change in lean loading does not reach the inlet of the absorber column until a delayed time due to the circulation times from stripper sump outlet to absorber inlet (in this case around 14 min with the solvent flow rate of Case 1 in Figure 3 and Table 3). In addition, the rise time required for the response in lean flow rate of around 6 min adds to a total delay of around 20 min in the recycle loop. Once the increase in solvent lean loading reaches the absorber column the Cap_B and CO_2 absorbed tends to decrease. In general, it can be said that the Cap_A (and CO_2 desorbed) reaches stabilization with a smoother trajectory (without significant inverse response). Note that Cap_B peaked at a value of 0.941 and Cap_A peaked at a value of 0.890. The inverse response is also shown in the transient response of the absorber temperature profile, refer to T_{a2} and T_{a3} in test C of Figure 6. However, the peak in temperature T_{a3} in the absorber column happened after around 33 min, which is a longer delay than capture rate. This could be due to the effects of thermal inertia in the absorber column. For solvent flow rate increase it can be observed that the stripper temperature profile was displaced towards relatively lower temperature values; refer to Figure 7 test C. This can explain the higher resulting desorption ratio in the stripper column. In addition, the response of stripper temperature profiles is faster (rise time of T_{s1} of around 4 min) than for absorber temperature profiles. The inverse response observed in test C was also observed in tests B (initial part of the test until around 22.30),

test E and test F. Analog explanations to test C could be written for the output trajectories observed in tests B, E and F for absorber temperature profiles, CO_2 absorbed and Cap_B. For all the tests with solvent flow rate change (B, C, E and F), the observed response of CO_2 desorbed and Cap_A was smother (without significant inverse response and with relatively larger peaking values) and faster (took less time to stabilize) than CO_2 absorbed and Cap_B, respectively. In addition, the stripper temperature profiles seem to stabilize faster than absorber temperature profiles for set-point step changes in solvent flow rate. The process stabilized after around 45 min for test C.

In test D, flue gas volumetric flow rate was increased from 47 000 Sm^3/hr to 60 000 Sm^3/hr, which corresponds with 78% to 100% flue gas volumetric flow rate capacity in the absorber column, respectively. The rise time for measured flue gas flow rate was 8 minutes; refer to Figure 4. During test D the rich and lean solvent flow rates remain constant, while small fluctuations were observed in steam flow rate to the reboiler and calculated reboiler duty. The capture rate changed significantly from around 86% to around 68%. In this case the trajectory of capture rate followed quite well the variation of flue gas volumetric flow rate, since the CO_2 mass flow rate fed to the absorber column is included in the calculation of capture rates (refer to Equations (1) and (2)). In addition, the change in flue gas flow rate does not significantly change the amount of CO_2 being absorbed at initial and final steady-state conditions, as observed in test A. As in test A, a significant change in volumetric flow rate had an impact on absorber temperature profiles, with a change in T_{a3} from around 47 °C to around 39 °C. In this case the response of T_{a3} to the change in flue gas flow rate had a time constant of 17 min and a rise time of around 34 min. This shows again the effects of thermal inertia of the process of heat and mass transfer in the absorber column to changes in flue gas volumetric flow rate. The stripper temperature profile remained constant during the tests A and D of step-change in flue gas flow rate, as shown in Figure 7. The transient trajectories of Cap_A and Cap_B stabilized after approximately 55 min.

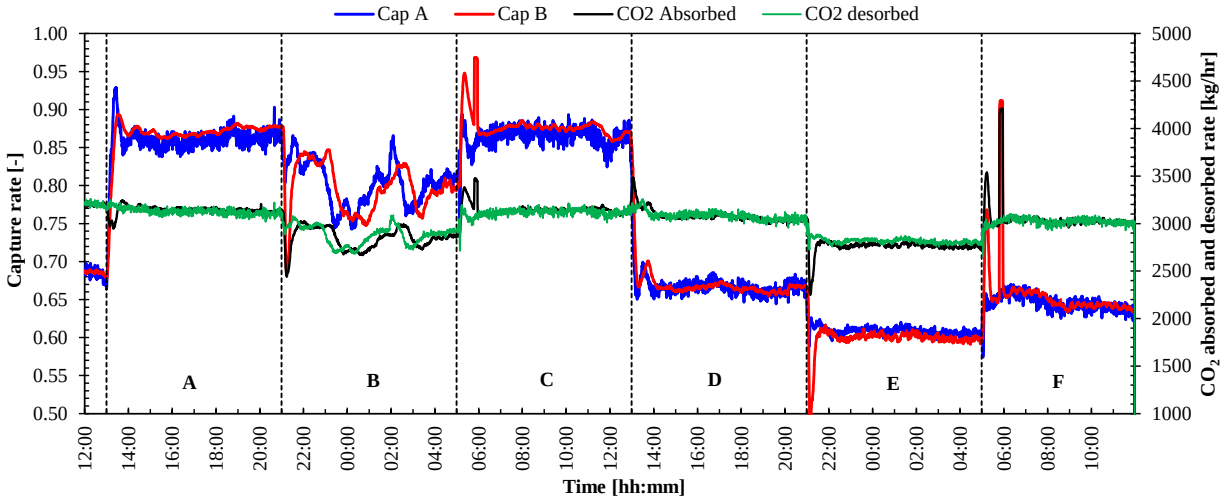

Figure 5. Transient response of capture rate Cap_A and Cap_B calculated as presented in equations (1) and (2), respectively. The open loop tests are shown for 48 hours of testing from July 21 to July 23. The vertical lines correspond to the time at which the set-point changes are applied for tests A to F as presented in Table 5.

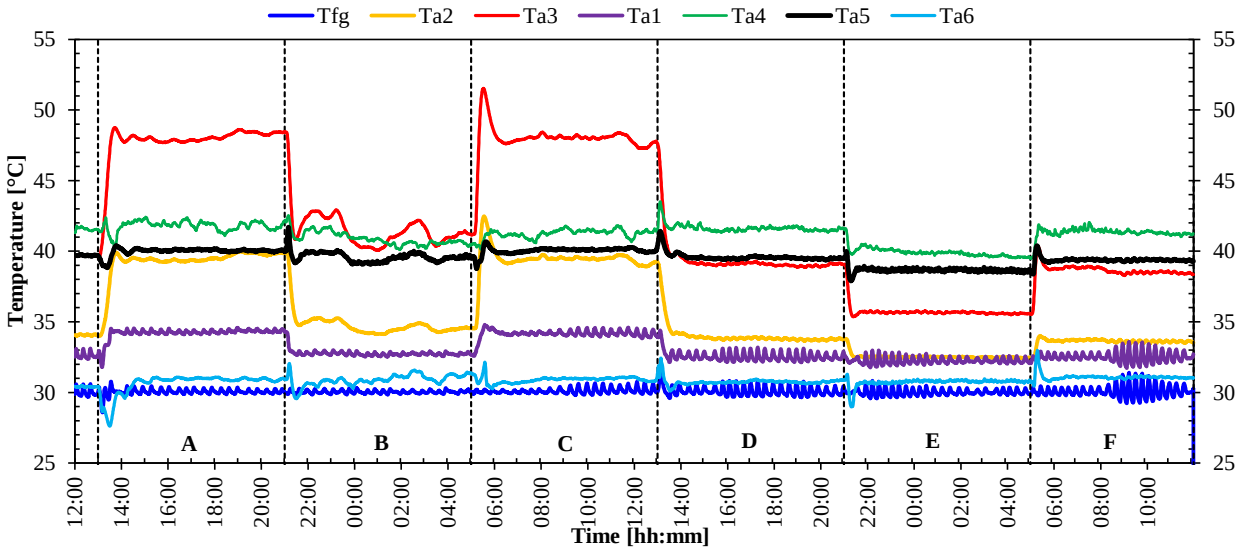

Figure 6. Transient response of absorber temperatures: T_{a1}, T_{a2}, T_{a3}, T_{a4} and T_{a5} and T_{a6} are temperatures at the inlet of the column, in between the different packing segments from bottom to top; refer to Figure 1. T_{fg} is the flue gas temperature at the inlet of the absorber column. The open-loop tests are shown for 48 hours of testing from July 21 to July 23. The vertical lines correspond to the time at which the set-point changes are applied for tests A to F as presented in Table 5.

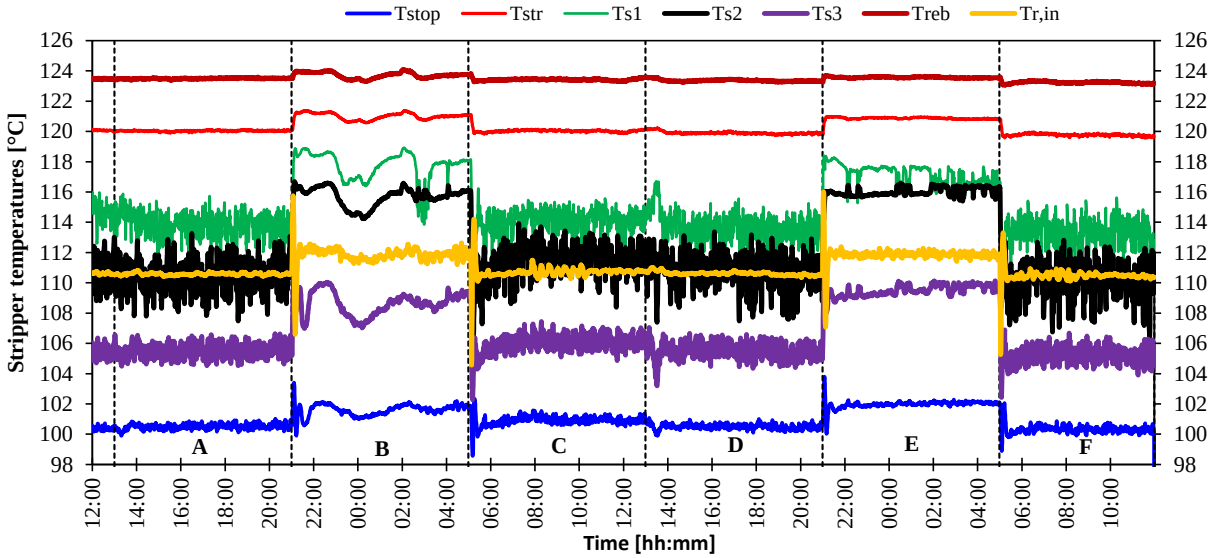

Figure 7. Transient response of stripper temperatures: T_{s1}, T_{s2} and T_{s3} are averaged stripper packed temperatures at the packing bottom, middle and top, respectively. T_{str} is the liquid temperature at stripper sump, T_{reb} is the reboiler solution temperature and T_{stop} is the stripper temperature at the top of the packing and $T_{r,in}$ is the rich solvent temperature at the inlet of the stripper column. The open-loop tests are shown for 48 hours of testing from July 21 to July 23. The vertical lines correspond to the time at which the set-point changes are applied for tests A to F as presented in Table 5.

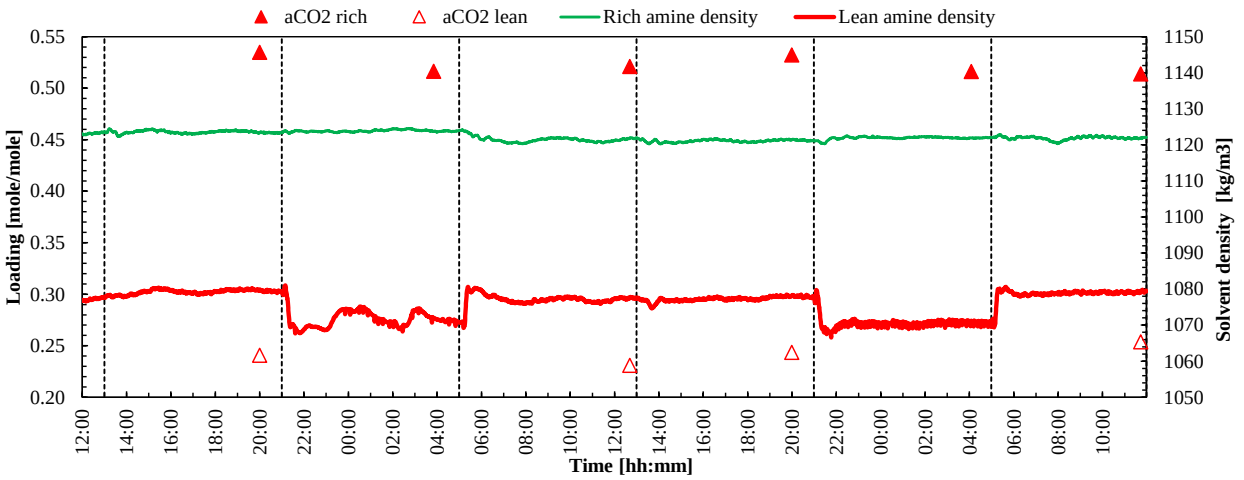

Figure 8. Transient response of lean and rich solvent densities; and values of lean and rich loading samples taken before the beginning of each test. The open-loop tests are for 48 hours of testing from July 21 to July 23. The vertical lines correspond to the time at which the set-point changes are applied for tests A to F as presented in Table 5.

4.2. Decentralized control structures

4.2.1. Control of liquid to gas ratio (*L/G*) and stripper bottom temperature (T_{str})

In this section, the results from the tests on fast load change with *L/G* ratio control are presented, refer to Table 6 in Section 2.3.1. In the figures included in this section, the vertical dotted line indicates the time at which the tests begin with the change in flue gas flow rate. Note that test 2 was stopped after 95 minutes, since it was considered that stabilization of process variables was achieved. Figure 9 shows the trajectories of volumetric flue gas flow rate (F_{gas}), rich solvent mass flow rate (F_{solv}), steam mass flow rate (F_{steam}) to the reboiler, the resulting *L/G* ratio in the absorber column, and the backpressure of the rich amine solvent pump. Figure 10 shows the trajectories for capture rates Cap_A and Cap_B, while Figure 11 shows the trajectories of stripper bottom temperature (T_{str}), CO_2 desorbed and CO_2 absorbed. In addition, Table 8 shows the resulting total stabilization times for CO_2 absorbed and CO_2 desorbed trajectories for tests 1 to 4. Here total stabilization times are calculated considering 10% settling times.

Figure 9a shows the trajectories of flue gas flow rate disturbances applied to the pilot plant for tests 1 to 4. In this case the operators changed directly the fan speed in order to achieve the desired ramp trajectory, instead of changing the flue gas flow rate controller F_{gas} set-point. This avoided the oscillatory behavior of the flue gas volumetric flow rate trajectory presented in test A, section 3.1. Figure 9b shows the trajectory of rich solvent flow rate. The set-point was changed with a ramp rate of 10%/min, and the resulting rise times vary from 3.5 to 5.5 min, refer to Table 6. In test A, marginally stable oscillations around the final set-point of 52 000 kg/hr were observed in the trajectory of rich solvent flow rate, from time 5 min to time 130 min. This was due to flashing of rich solvent. In Figure 9e oscillations of rich pump backpressure during test 1 are shown. To solve this problem, the operator increased the backpressure of the rich pump by throttling a valve located in the hot side of the rich piping between lean/rich heat exchanger and stripper column; refer to rich pump backpressure in test 1 from 130 min to 170 min in Figure 9e. In following tests

2, 3 and 4 the operator manipulated this valve opening in order to avoid flashing and the consequent oscillation in the rich flow rate (and lean solvent flow rate); refer to Figure 9.

Table 8. Total stabilization times [min] for CO_2 desorbed and CO_2 absorbed trajectories for tests 1-8. The trajectories were calculated considering the 10% settling time, and for disturbances in flue gas volumetric flow rate.

Stabilization times [min]	Test 1	Test 2	Test 3	Test 4	Test 5	Test 6	Test 7	Test 8
CO_2 Desorbed	45	26	-	41	-	41	48	48
CO_2 Absorbed	53	37	-	63	-	49	68	107

Test 1 consisted of a reduction of flue gas flow rate from 60 000 Sm^3/hr to 47 000 Sm^3/hr, and the solvent flow rate was reduced to keep *L/G* ratio to a value of around 1.04 kg/Sm^3. Due to the solvent flashing phenomena, the *L/G* ratio in the absorber column oscillated around the final steady-state value; refer to Figure 9d. This lead to small amplitude oscillations around the final steady-state for all the process variables shown in Figure 10 and Figure 11, and it can be considered that the process achieved conditions of marginal stability. Considering the averaged value of CO_2 absorbed and CO_2 desorbed once the marginal stability was achieved, the total stabilization time was longer for CO_2 absorbed (53 min) than for CO_2 desorbed (45 min); refer to Table 8. In addition, it seems that Cap_A reaches stabilization faster than Cap_B. However, the trajectory of Cap_A was more sensitive to the disturbance and peaked at a value of 1.05 at time 5 min (see Figure 10a), while Cap_B peaked at a value of 0.90 at 8.5 min; refer to Figure 10b. A capture rate value of Cap_A higher than 1 means that there is more CO_2 being desorbed than what is being fed to the process, during the transient conditions. This high peak can be explained by the dead time observed on steam flow rate in Figure 9c (around 5 min), due to the fact that there is a dead time of around 3 min for a significant change to be observed in the stripper bottom temperature (T_{str}). Once the stripper bottom temperature began to increase due to the lower amount of solvent being sent to the stripper, the T_{str} controllers reduced the solvent flow rate sent to the reboiler. The temperature controller kept the T_{str} close to the desired set point of 120.9 °C without excessive variations (<1 °C). Despite of the marginal stable behavior due to solvent flashing, the process can reject the disturbance and it reached stabilization within 55 min.

Test 2 was a test for fast load change with a flue gas flow rate increase from 47 000 Sm^3/hr to 60 000 Sm^3/hr; refer to Table 6. In addition, *L/G* ratio was kept constant to a value of around 1.04 kg/Sm^3 by a ramp up of rich solvent flow rate; refer to Figure 9b. As for the case on load reduction (test 1), it took longer for the trajectory of CO_2 absorbed to stabilize (37 min) than CO_2 desorbed (26 min); refer to Table 8. Cap_A was again more sensitive to the disturbance with a peak down at value of 0.56 at time 2.5 min (refer to Figure 10a), while Cap_B peaked down at 0.65 at time 3 min. In addition, the temperature of the stripper is controlled to 120.9 °C without excessive excursions (<1.2 °C). The process can reject the disturbance of flue gas flow rate change and can bring the process towards stable desired steady-state conditions within 37 min. This was significantly faster than for load reduction in test 1, that took 55 min (refer to Table 8). This suggests that it can be faster to reach stabilization and to reject disturbances when ramping up the volumetric flow rate than when ramping it down.

Test 3 consisted of a reduction of flue gas volumetric flow rate from 60 000 Sm^3/hr to 36 000 Sm^3/hr (corresponding to 100% to 60% flue gas volumetric capacity in absorber column). The solvent flow rate was reduced in order to keep *L/G* ratio at a value of around 1.05 kg/Sm^3 in the absorber column; refer to Figure 9d. The inputs to the process F_{gas} and F_{solv} reached stabilization, with a rise time of 6 minutes. However, significant instabilities were found in the steam mass flow rate sent to the reboiler (F_{steam}) which oscillated around the value of 3 600 kg/hr and had initial peaks of 2 540 kg/hr at time 20 min and 5 130 kg/hr at time 32 min; refer to Figure 9c. The large reduction in solvent flow rate (F_{solv}) resulted in a significant disturbance to the flow network. Fluctuations in the steam flow rate resulted in significant fluctuations of Cap_A and Cap_B (see Figure 10), CO_2 absorbed, CO_2 desorbed and stripper bottom temperature (T_{str}) (see Figure 11). This was due to the stripper temperature controller, which was very sensitive to changes in stripper bottom temperature (T_{str}). This suggests that the value of the controller gain was too large. Actually, oscillation disappeared when the operator set the temperature controller on manual and setting a given value of steam flow rate (not shown). Again, Cap_A and desorbed CO_2 were more sensitive to the fluctuations of steam flow rate than Cap_B and CO_2 absorbed, as can be observed in Figure 10a and Figure 11a. Comparing with test 1, for larger disturbances in flue gas volumetric flow rate it can be more complicated to reject the disturbance and reach stabilization of the process variables with feedback control. This suggests that further work should be done at the TCM amine pilot plant to fine tune the controllers of the regulatory control layer of the process, if large and fast disturbances in flue gas flow rate are to be rejected.

Test 4 shows a flue gas volumetric flow increase from 36 000 Sm^3/hr to 60 000 Sm^3/hr with a rise time of 5 min, which represents 60% to 100% of absorber flue gas volumetric flow rate capacity. Rich solvent flow rate (F_{solv}) was increased from 45 000 kg/hr to 65 000 kg/hr with a rise time of 5 min, in order to keep the *L/G* ratio at a value of around 1.03 kg/Sm^3 at the initial and final steady-state operating conditions. It can be observed how steam flow rate saturated (reached a maximum value of 6 560 kg/hr) from around t=25 min to around t=35 min; refer to Figure 9c. Input saturation is not desired in control for smooth operation of the process. This suggests that the controller gain for the T_{str} controller is too large, and that the stripper temperature set-point was too large for the given process conditions. However, at time t=35 min the steam mass flow rate was reduced by the action of the steam temperature controller. The operators considered that the process achieved stabilization at around time t = 70 min, and injected liquid water in the steam supply line to avoid excessive temperature of the supply superheated steam (limited to 150 °C) according to TCM pilot plant operation guidelines. This reduced the available heat and the resulting stripper bottom temperature (T_{str}). However, it can be considered that the process stabilized at around 70 min. CO_2 desorbed stabilized faster (41 min) than CO_2 absorbed (63 min); refer to Table 8.

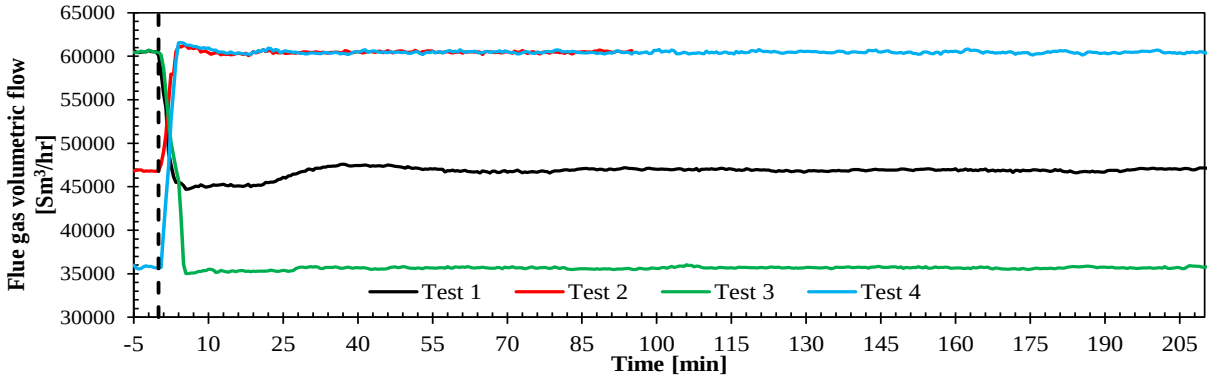

a)Flue gas volumetric flow rate [Sm^3/hr]

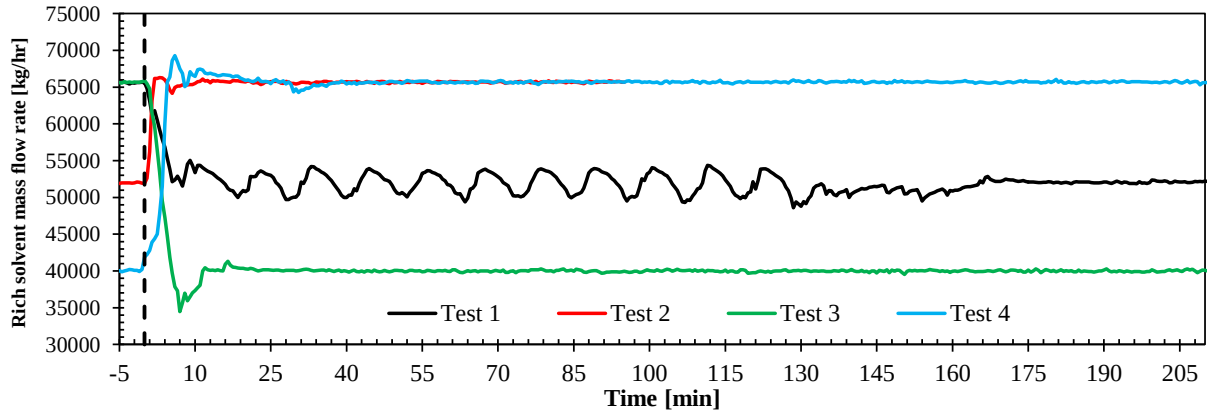

b) Rich solvent mass flow rate [kg/hr]

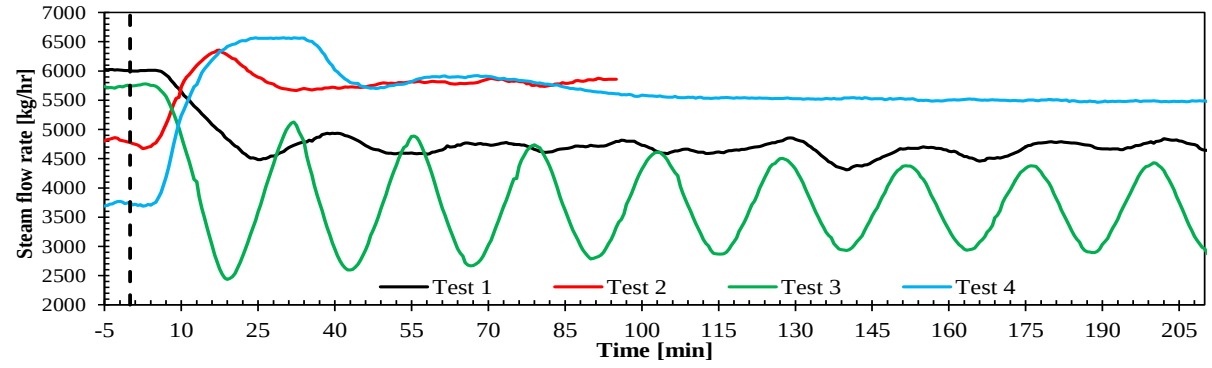

c) Steam flow rate [kg/hr]

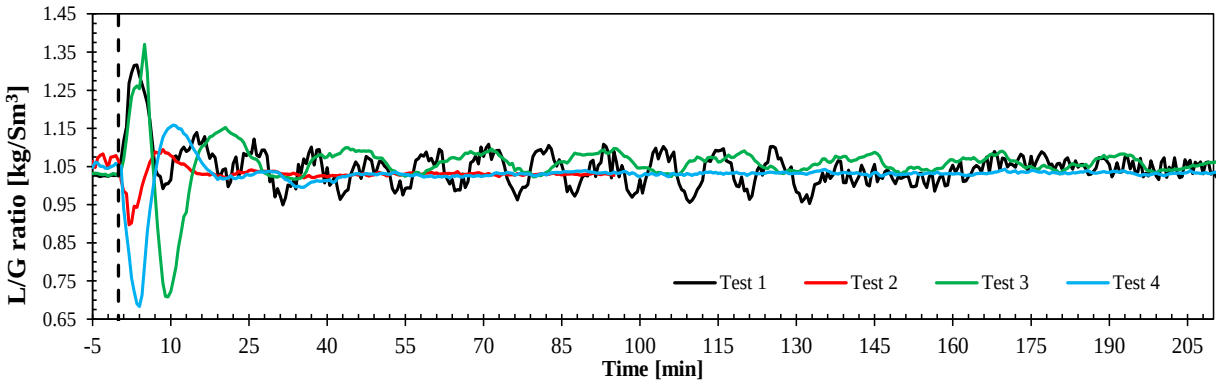

d) L/G ratio [kg/Sm³]

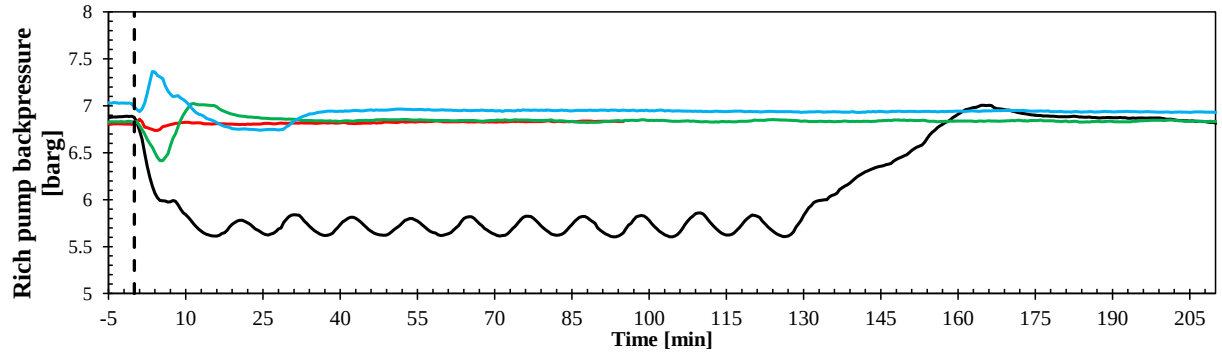

e) Backpressure of rich amine pump [barg]

599 **Figure 9. Experimental results for tests on load change driven by flue gas flow rate reduction and increase for tests 1 to 4**
600 **in Table 6. The process variables measured are the main inputs to the amine plant during the tests.**

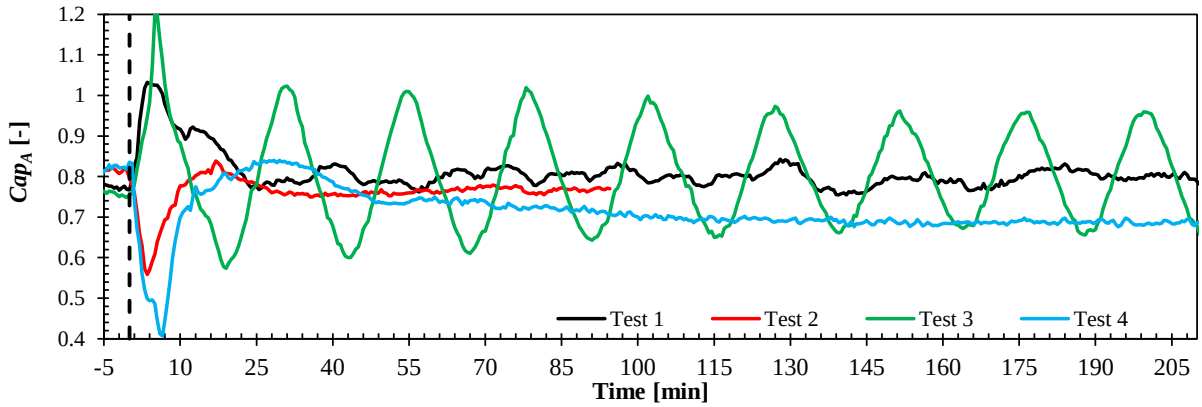

a) Capture rate Cap_A

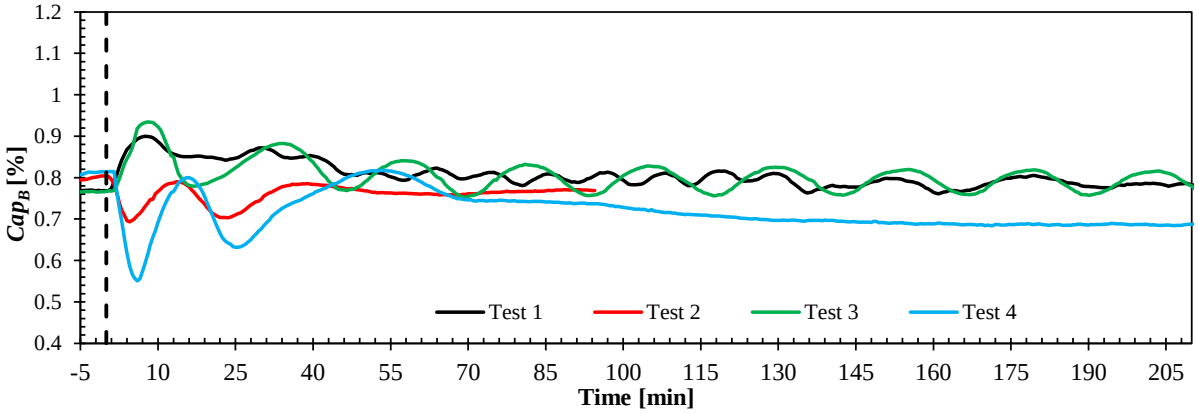

b) Capture rate Cap_B

Figure 10. Experimental results for tests 1, 2, 3 and 4 in Table 6. Capture rates Cap_A and Cap_B calculated as in equations (1) and (2), respectively. Capture rates are shown for the four transient events in which L/G ratio is kept constant by manipulating the solvent flow rate in order to keep constant the L/G ratio.

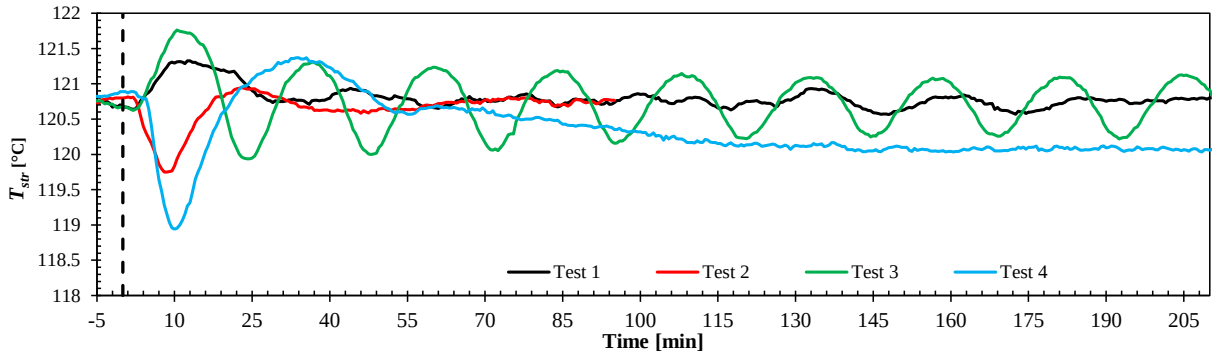

a) Stripper bottom temperature [°C]

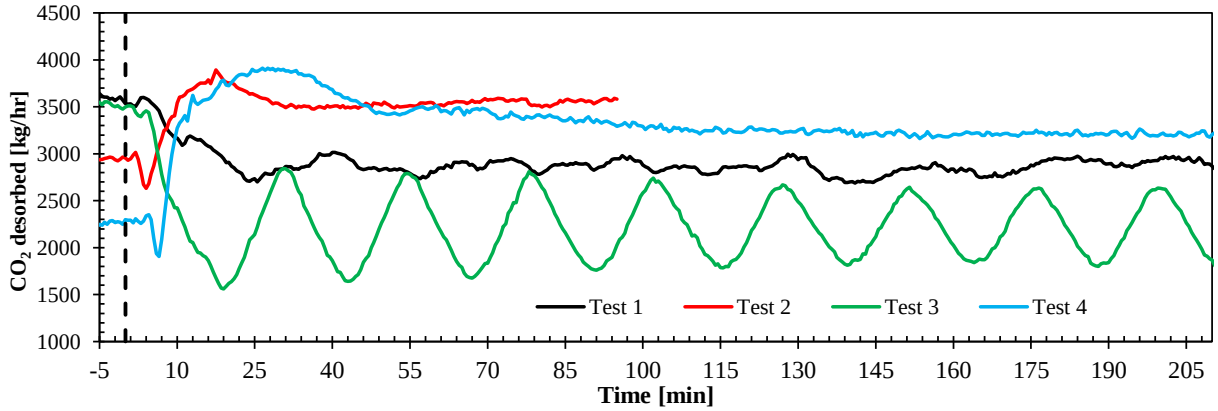

b) CO_2 desorbed [kg/hr]

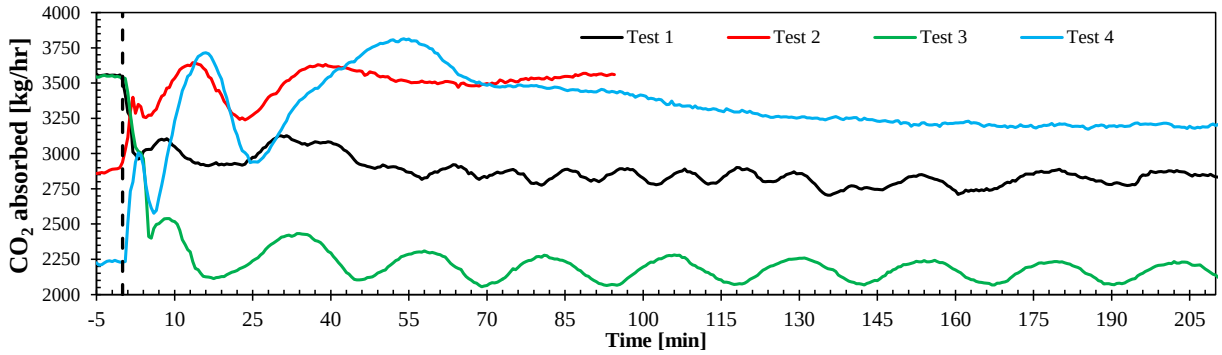

c) CO_2 absorbed [kg/hr]

Figure 11. Experimental results for tests 1, 2, 3 and 4 in Table 6. Stripper bottom temperature, CO_2 desorbed and CO_2 absorbed during transient load changes of the amine plant.

4.2.2. Control of capture rate Cap_A

In this section the results from the tests on fast load change with CO_2 capture rate control are presented, refer to Table 7 in section 2.3.2. In the figures included in this section, the vertical dotted lines indicate the time at which the tests begin with the change in flue gas flow rate. Note that test 6 was stopped after 140 minutes because it was considered that the plant was operated under steady-state conditions. Figure 12 shows the trajectories of flue gas volumetric flow rate (F_{gas}), rich solvent mass flow rate (F_{solv}), steam mass flow rate (F_{steam}) to the reboiler and the resulting *L/G* ratio in the absorber column. Figure 13 shows the trajectories for capture rates Cap_A and Cap_B, while Figure 14 shows the trajectories of stripper bottom temperature (T_{str}), CO_2 desorbed and CO_2 absorbed. In addition, Table 8 shows the resulting total stabilization times for CO_2 absorbed and CO_2 desorbed trajectories for tests 5 to 8.

Test 5 consisted of a reduction of flue gas flow rate from 60 000 Sm^3/hr to 47 000 Sm^3/hr; refer to Figure 12a. Solvent flow rate was set to control capture rate Cap_A to a set point of 0.74, and steam flow rate was set to control stripper bottom temperature (T_{str}) to a value of 120.5 °C. The manipulated variables of the controller layer F_{solv} and F_{steam} are shown in Figure 12b and Figure 12d. It can be seen that the solvent flow rate was reduced by the controller after the disturbance was introduced, with a dead time of around 7 minutes. At time t=32 min, the solvent flow rate began to increase and started to have small amplitude oscillations. As observed in the trajectory of Cap_A (in Figure 13a), at the initial part of the transient (from time t=0 min to time t=45 min) the controller brought the process Cap_A towards the target set point, however from time t=50 min the trajectory of Cap_A showed an oscillatory trajectory with increasing amplitude. As in test 3, solvent flow rate (F_{solv}) variations induced variations in the stripper bottom temperature, hence the steam sent to reboiler was modified by the T_{str} controller, resulting in an oscillatory trajectory with growing amplitude of F_{steam}. Since Cap_A is sensitive to changes in F_{steam}, the capture rate trajectory Cap_A will follow the variations in F_{steam}. Then, the controller of Cap_A modifies further solvent flow rate, resulting in the unstable behavior of the process. At the time around t=150 min, the operator disconnected the T_{str} controller and set a given value of steam pressure, and the oscillatory behavior stopped, bringing the process towards steady-state conditions. This test illustrates the interaction between the feedback control loops, that results in unstable performance of the process in response to the disturbance in flue gas flow rate reduction. In addition, this test shows the challenge of tuning the feedback controllers of the process if decentralized

control structures are to be applied to control the chemical absorption process for fast load change disturbances, especially when ramping down the flue gas volumetric flow rate capacity.

Test 6 shows a transient test on load change increase by implementing an increase in flue gas volumetric flow rate from 47 000 Sm^3/hr to 60 000 Sm^3/hr. The same control structure as the one utilized in test 5 was implemented; refer to Table 7. In this case the control structure managed to bring the process towards the desired steady-state operating conditions after the disturbance in flue gas volumetric flow rate was applied to the process; refer to Figure 12a. CO_2 desorption rate required a total stabilization time of 41 min, and stabilized faster than CO_2 absorption rate CO_2 (49 min). This test contributed to emphasize that ramping up flue gas flow rate towards full capacity (or close to design conditions) is less challenging than ramping down flue gas flow rate (towards steady-state off-design conditions within the operating window of the process). In addition, the disturbance in CO_2 vol% from a value of 4.1 to 3.7 happened at time t=72 min with a rise time of 6 minutes; refer to Figure 2. This disturbance affects significantly the Cap_A output trajectory, which increases instantaneously, since the amount of CO_2 fed to the process is reduced due to this disturbance; refer to Figure 13a at time t=72 min. However, it seems that the buffering effect of the process to disturbances at the inlet to the plant avoids a significant change in the trajectories of the rest of process variables presented in this section, and hence the disturbance in terms of CO_2 vol% is properly rejected with this control structure.

Test 7 shows the response of the process when operated with control structure in which Cap_A is controlled by manipulating solvent flow rate F_{solv}, and in this case steam flow rate is reduced by applying a ramp from around 5 300 kg/hr to 4 000 kg/hr in 40 min. This ramp was specified based on the steam flow rate trajectory during the first 50 min of transient test 5, in order to test the response of the process when steam flow rate was operated with a feedforward action by modifying the steam pressure (disconnecting the T_{str} feedback control loop). Note that during test 7 the initial conditions were significantly different than those for test 5. Even if both had 100% volumetric flow rate in the absorber column (refer to Figure 12a time t=-5 min to t=0 min), the initial process conditions in terms of F_{solv}, and F_{steam} were different in order to reach a similar Cap_B value of 0.74; refer to Figure 13b. In addition, this could be explained by the lower CO_2 content during test 7 (3.7 vol%) than for test 1 (4.1 vol%), since lower amount of CO_2 needs to be absorbed and desorbed in the absorber and stripper column; refer to time t=-5 to time t=0 minutes in Figure 14. It can be seen that for test 7 oscillations and instabilities are not found as for the similar test 5 when ramping down flue gas flow rate. This confirmed that the control loop triggering the instabilities was the stripper bottom temperature (T_{str}) controller during test 5. The CO_2 desorbed stabilizes after around 48 minutes, while CO_2 absorbed took 68 minutes; refer to Table 8. The final steady-state conditions result in a larger L/G ratio of around 1.15 kg/Sm^3 (refer to test 7 in Figure 12d), and lower stripper bottom temperature (T_{str}), refer to Figure 14a.

Test 8 shows the response of the process when operated with control structure in which Cap_A is controlled by manipulating solvent flow rate (F_{solv}), and steam flow rate was increased by applying a ramp from around 4 000 kg/hr to 5 300 kg/hr in 40 min. This ramp was specified based on the steam flow rate trajectory during the first 50 min of transient test 6, in order to test the response of the process when steam flow rate was operated with a feedforward action by modifying the steam pressure (disconnecting the T_{str} feedback control loop). The controller managed to control the capture rate Cap_A and stabilized the plant without significant oscillations after around 107 min (refer to CO_2 absorbed in Table 8 and Figure 14). Therefore, the process

675 stabilized faster when using feedback control for T_{str} (in test 6). The resulting final steady-state process
676 conditions presented a relatively low *L/G* ratio (Figure 12d) and larger stripper bottom temperature (T_{str}).

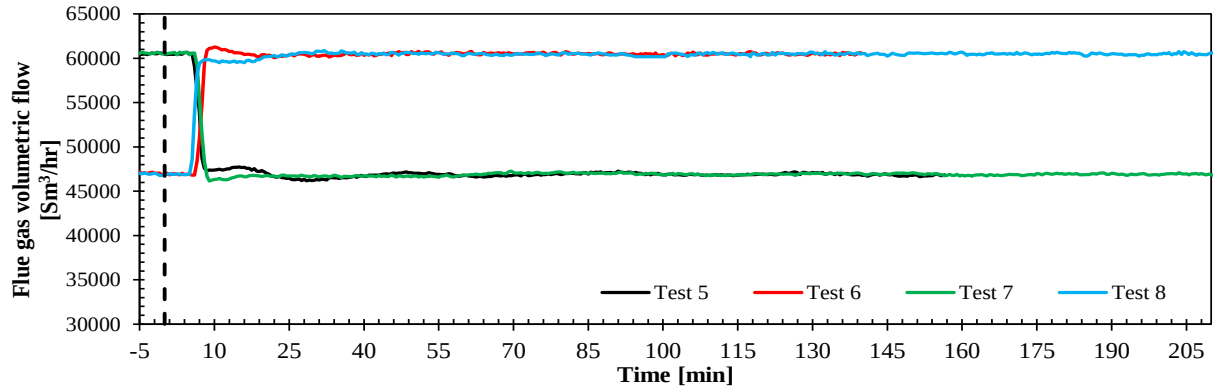

a) **Flue gas volumetric flow rate [Sm³/hr]**

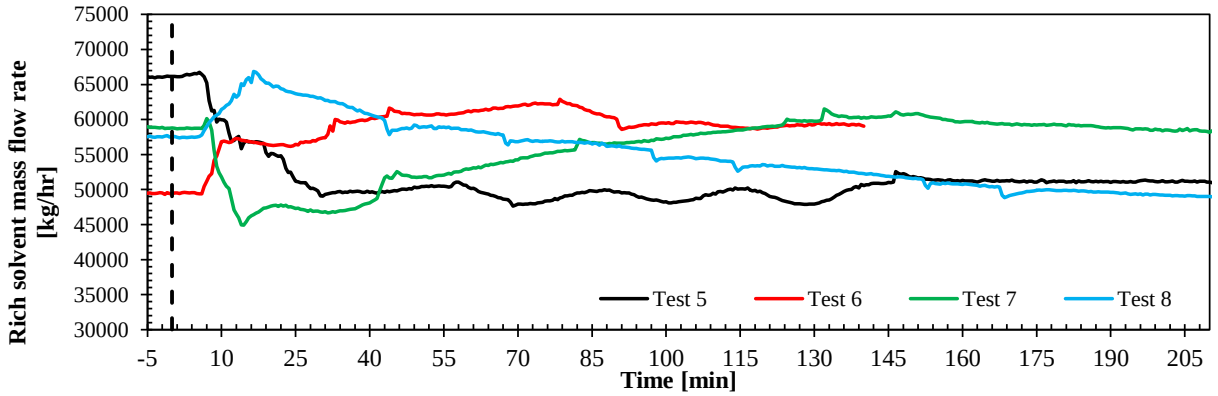

b) **Rich solvent mass flow rate [kg/hr]**

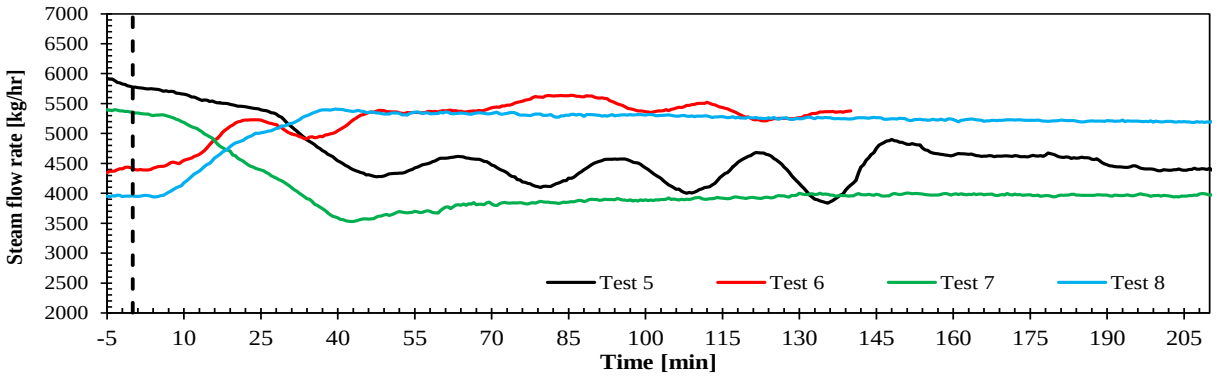

c) **Steam flow rate [kg/hr]**

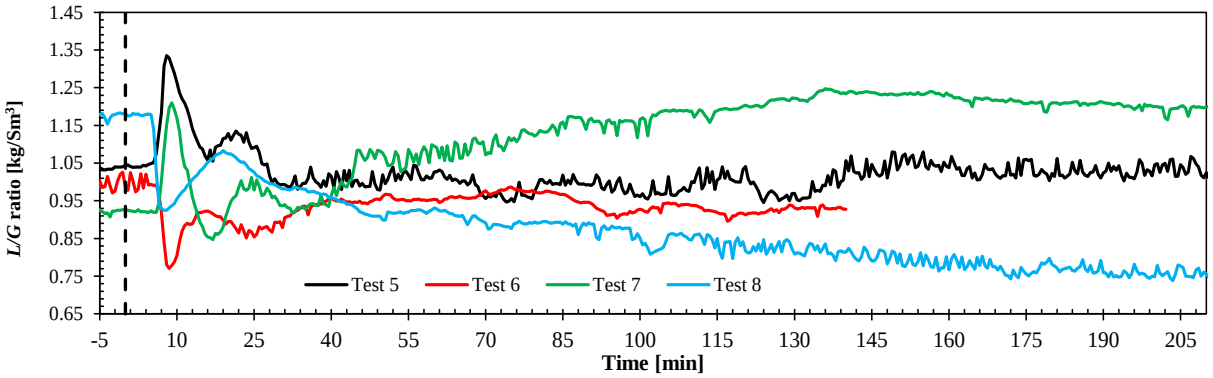

d) **L/G ratio [kg/Sm3]**

677 **Figure 12. Experimental results for tests on load change driven by flue gas flow rate reduction and increase. The process**
678 **variables measured are the main inputs to the amine plant during the tests. The control structure tries to keep constant the**
679 **capture rate in absorber column by manipulating rich solvent flow rate, refer to Table 7.**

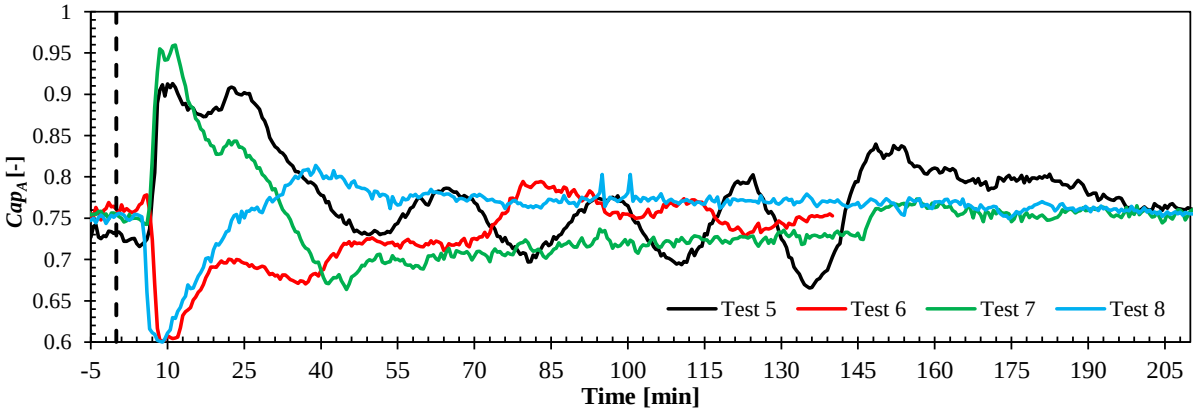

a) **Capture rate *Cap*$_A$**

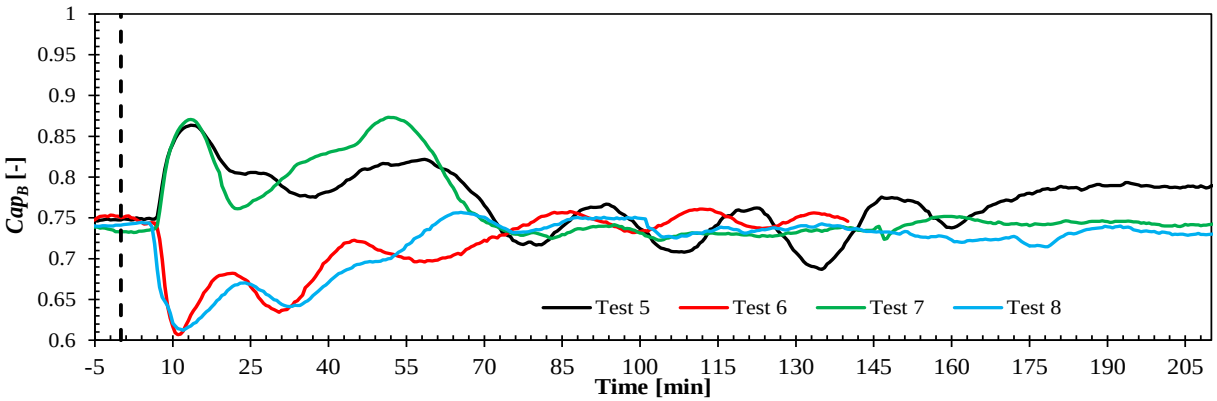

b) **Capture rate *Cap*$_B$**

680 **Figure 13. Experimental results for tests 5, 6, 7, and 8 in Table 7. Absorption and desorption rates are shown for the four**
681 **transient events in which L/G ratio is kept constant by manipulating the solvent flow rate in order to keep constant the L/G**
682 **ratio.**

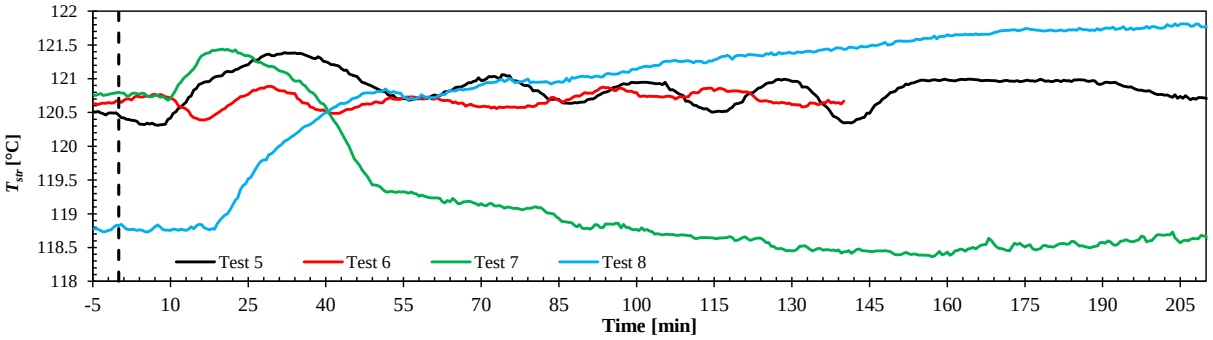

a) Stripper bottom temperature [°C]

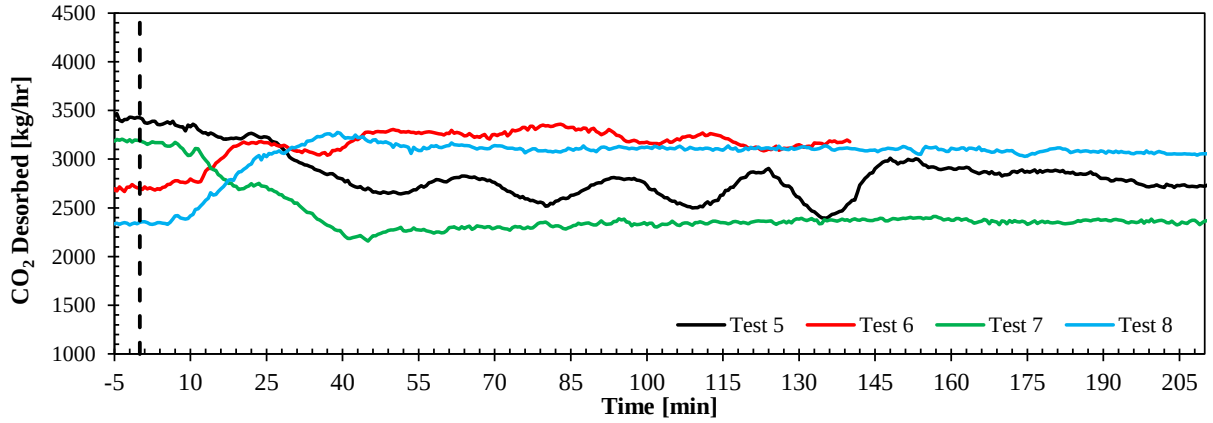

b) CO_2 desorbed [kg/hr]

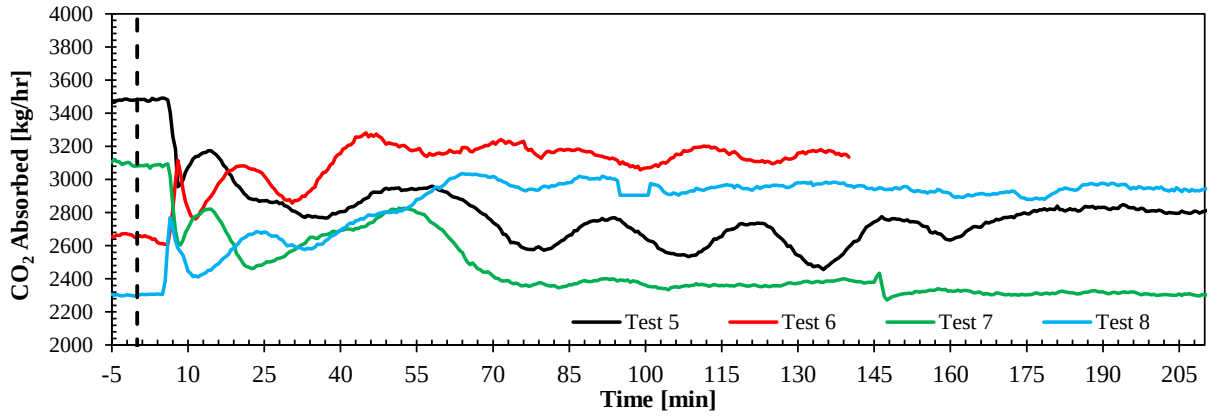

c) CO_2 absorbed [kg/hr]

683 **Figure 14. Experimental results for tests 5, 6, 7 and 8 in Table 7. Stripper bottom temperature T_{str}, CO_2 desorbed and CO_2**
684 **absorbed during transient load changes of the amine plant.**

685

5. Conclusions

Tests on open-loop responses of the plant revealed that for step changes in flue gas volumetric flow rate the absorption and desorption rate did not change significantly from initial to final steady-state conditions. While the absorber temperature profiles are affected by changes in volumetric flow rate, the stripper temperature profile remains approximately constant with same values for the step changes in flue gas flow rate applied in test A and D. For changes in flue gas flow rate the process will take a maximum of around 55 min to stabilize. Changes in steam flow rate to reboiler showed that desorption rates are sensitive to changes in reboiler duty, and CO_2 desorption rate follows tightly the changes in steam flow rate, while the CO_2 absorption rate response follows with a delay due to circulation times in the recycle loop. The stripper process conditions change relatively fast in response to inputs of steam flow rate, while the response of the performance of the absorber column is slower. In addition, for step changes in rich solvent flow rate the solvent flow network stabilizes within 6 minutes, which is faster compared to rest of process variables. When the capture rate is defined with the absorption rate Cap_B, the output trajectory describes a slow inverse response due to solvent circulation times through the recycle loop, while the capture rate Cap_A defined with CO_2 desorbed reaches stabilization without a significant inverse response. For all tests with solvent flow rate it took less time to stabilize CO_2 desorbed than CO_2 absorbed (around 45 min in test C).

Tests for fast load change scenarios applied to the pilot plant revealed that the process can reject fast disturbances in flue gas flow rate and could bring the process towards desired off-design steady-state conditions within 60 min by employing decentralized control structures. These tests provide empirical evidence at demonstration scale that combined cycle power plants with post combustion CO_2 capture can keep similar operational procedures as equivalent unabated power plants, considering fast cycling load changes driven by fast GT load change. However, care must be taken when tuning the feedback control loops of the process and especially of the regulatory control layer. Further work at TCM DA is required to tune the controllers of the regulatory control layer of the amine plant so that faster closed-loop responses are achieved, allowing for tighter control of process variables in the advanced control layer.

Large load changes from maximum to minimum online operation flue gas volumetric flow rate (100% to 60% volumetric flow rate) in the pilot plant can cause instabilities due to the low rich solvent flow. At low solvent flow rates (desired at low loads for efficient off-design steady-state operation of the plant) the circulation times within process equipment increases, slowing the plant response to change in solvent flow rate and hence making more difficult to achieve tight control of capture rate Cap_A and stripper bottom temperature (T_{str}). In response to flue gas flow rate disturbance, fast and large changes in solvent flow rate as a control measure can cause instabilities due to the interaction between the stripper temperature and the capture rate control loops. Unintended disturbances in CO_2 vol% showed the importance of feedback control in order to keep the plant within desired steady-state operating conditions. A combination of feedforward and feedback algorithms could be a solution to achieve fast and stable disturbance rejection.

Acknowledgements

The authors acknowledge the Department of Energy and Process Engineering at NTNU-Norwegian University of Science and Technology and TCM DA owners Gassnova, Shell, Statoil, Sasol and Total, for funding this project.

Symbols and abbreviations

3PRH	Three pressure reheat
CCS	Carbon capture and storage
CHP	Combined heat and power
F_{gas}	Flue gas volumetric flow rate [Sm^3/hr]
F_{prod}	CO_2 product mass flow rate [kg/hr]
F_{solv}	Rich solvent mass flow rate [kg/hr]
F_{steam}	Reboiler steam mass flow rate [kg/hr]
Cap	Capture rate
DCC	Direct contract cooler
GT	Gas turbine
L/G	Liquid to gas ratio [kg/Sm^3]
MEA	Monoethanolamine
PCC	Post combustion CO_2 capture
PI	Proportional-Integral feedback controller
SIMC	Simple internal model control
SRD	Specific reboiler duty [kJ/kg CO_2]
T_{str}	Stripper bottom temperature [°C]
TCM DA	Technology Centre Mongstad
TPM	Throughput manipulator

References

[1] IPCC, Climate Change 2014: Synthesis Report. Contribution of Working Groups I, II and III to the Fifth Assessment Report of the Intergovernmental Panel on Climate Change, in, IPCC, Geneva, Switzerland, 2014, pp. 151 pp.

[2] IEA, CO2 Capture and storage: A key carbon abatement option, in: Energy Technology Analysis, International Energy Agency, 2008.

[3] IEA, World Energy Investment 2016, in, 2016.

[4] M.E. Boot-Handford, J.C. Abanades, E.J. Anthony, M.J. Blunt, S. Brandani, N. Mac Dowell, J.R. Fernandez, M.-C. Ferrari, R. Gross, J.P. Hallett, R.S. Haszeldine, P. Heptonstall, A. Lyngfelt, Z. Makuch, E. Mangano, R.T.J. Porter, M. Pourkashanian, G.T. Rochelle, N. Shah, J.G. Yao, P.S. Fennell, Carbon capture and storage update, Energy & Environmental Science, 7 (2014) 130-189.

[5] A. Singh, K. Stéphenne, Shell Cansolv CO2 capture technology: Achievement from First Commercial Plant, Energy Procedia, 63 (2014) 1678-1685.

[6] N.E.T. Laboratory, Petra Nova Parish Holdings. W.A. Parish Post-Combustion CO2 Capture and Sequestration Project, in.

[7] NETL, Impact of Load Following on Power Plant Cost and Performance, in, 2012.

[8] M.A. Gonzalez-Salazar, T. Kirsten, L. Prchlik, Review of the operational flexibility and emissions of gas- and coal-fired power plants in a future with growing renewables, Renewable and Sustainable Energy Reviews, (2017).

[9] Lew; D., Brinkman; G., Kumar; N., Besuner; P., Agan; D., L. S., Impacts of Wind and Solar on Fossil-fueled Generators, in: IEEE Power and Energy Society General Meeting, San Diego, California, 2012.

[10] IEAGHG, Operating Flexibility of Power Plants with CCS, in, IEAGHG, June 2012.

[11] R.M. Montañés, M. Korpås, L.O. Nord, S. Jaehnert, Identifying Operational Requirements for Flexible CCS Power Plant in Future Energy Systems, Energy Procedia, 86 (2016) 22-31.

[12] M.S. Walters, T.F. Edgar, G.T. Rochelle, Regulatory Control of Amine Scrubbing for CO2 Capture from Power Plants, Industrial & Engineering Chemistry Research, 55 (2016) 4646-4657.
[13] S.Ó. Garðarsdóttir, R.M. Montañés, F. Normann, L.O. Nord, F. Johnsson, Effects of CO2-Absorption Control Strategies on the Dynamic Performance of a Supercritical Pulverized-Coal-Fired Power Plant, Industrial & Engineering Chemistry Research, 56 (2017) 4415-4430.
[14] R. M. Montañés, S.Ó. GarÐarsdóttir, F. Normann, F. Johnsson, L.O. Nord, Demonstrating load-change transient performance of a commercial-scale natural gas combined cycle power plant with post-combustion CO2 capture, International Journal of Greenhouse Gas Control, 63 (2017) 158-174.
[15] A. van de Haar, C. Trapp, K. Wellner, R. de Kler, G. Schmitz, P. Colonna, Dynamics of Postcombustion CO2 Capture Plants: Modeling, Validation, and Case Study, Industrial & Engineering Chemistry Research, 56 (2017) 1810-1822.
[16] K. Wellner, T. Marx-Schubach, G. Schmitz, Dynamic Behavior of Coal-Fired Power Plants with Postcombustion CO2 Capture, Industrial & Engineering Chemistry Research, 55 (2016) 12038-12045.
[17] Q. Zhang, R. Turton, D. Bhattacharyya, Development of Model and Model-Predictive Control of an MEA-Based Postcombustion CO2 Capture Process, Industrial & Engineering Chemistry Research, 55 (2016) 1292-1308.
[18] R. Dutta, L.O. Nord, O. Bolland, Selection and design of post-combustion CO2 capture process for 600 MW natural gas fueled thermal power plant based on operability, Energy, 121 (2017) 643-656.
[19] M. Bui, I. Gunawan, V. Verheyen, P. Feron, E. Meuleman, S. Adeloju, Dynamic modelling and optimisation of flexible operation in post-combustion CO2 capture plants—A review, Computers & Chemical Engineering, 61 (2014) 245-265.
[20] R. Faber, M. Köpcke, O. Biede, J.N. Knudsen, J. Andersen, Open-loop step responses for the MEA post-combustion capture process: Experimental results from the Esbjerg pilot plant, Energy Procedia, 4 (2011) 1427-1434.
[21] J. Åkesson, C.D. Laird, G. Lavedan, K. Prölß, H. Tummescheit, S. Velut, Y. Zhu, Nonlinear Model Predictive Control of a CO2 Post-Combustion Absorption Unit, Chemical Engineering & Technology, 35 (2012) 445-454.
[22] J. Gaspar, A. Gladis, J.B. Jørgensen, K. Thomsen, N. von Solms, P.L. Fosbøl, Dynamic Operation and Simulation of Post-Combustion CO2 Capture, Energy Procedia, 86 (2016) 205-214.
[23] N. Enaasen Flø, H. Knuutila, H.M. Kvamsdal, M. Hillestad, Dynamic model validation of the post-combustion CO2 absorption process, International Journal of Greenhouse Gas Control, 41 (2015) 127-141.
[24] R.M. Montañés, N.E. Flø, R. Dutta, L.O. Nord, O. Bolland, Dynamic Process Model Development and Validation with Transient Plant Data Collected from an MEA Test Campaign at the CO2 Technology Center Mongstad, Energy Procedia, 114 (2017) 1538-1550.
[25] N. Enaasen, L. Zangrilli, A. Mangiaracina, T. Mejdell, H.M. Kvamsdal, M. Hillestad, Validation of a Dynamic Model of the Brindisi Pilot Plant, Energy Procedia, 63 (2014) 1040-1054.
[26] A.S. Chinen, J.C. Morgan, B.P. Omell, D. Bhattacharyya, D.C. Miller, Dynamic Data Reconciliation and Model Validation of a MEA-Based CO2 Capture System using Pilot Plant Data, 11th IFAC Symposium on Dynamics and Control of Process Systems, including Biosystems, (2016).
[27] M. Bui, I. Gunawan, V. Verheyen, P. Feron, E. Meuleman, Flexible operation of CSIRO's post-combustion CO2 capture pilot plant at the AGL Loy Yang power station, International Journal of Greenhouse Gas Control, 48 (2016) 188-203.
[28] X. Zhang, X. Zhang, H. Liu, W. Li, M. Xiao, H. Gao, Z. Liang, Reduction of energy requirement of CO2 desorption from a rich CO2-loaded MEA solution by using solid acid catalysts, Applied Energy, 202 (2017) 673-684.
[29] H. Liu, H. Gao, R. Idem, P. Tontiwachwuthikul, Z. Liang, Analysis of CO2 solubility and absorption heat into 1-dimethylamino-2-propanol solution, Chemical Engineering Science, 170 (2017) 3-15.
[30] P. Tait, B. Buschle, I. Ausner, P. Valluri, M. Wehrli, M. Lucquiaud, A pilot-scale study of dynamic response scenarios for the flexible operation of post-combustion CO2 capture, International Journal of Greenhouse Gas Control, 48 (2016) 216-233.
[31] IEAGHG, Evaluation of process control strategies for normal, flexible, and upset operation conditions of CO2 post combustion capture processes. 2016/07, in, IEAGHG, September 2016.
[32] T. Nittaya, P.L. Douglas, E. Croiset, L.A. Ricardez-Sandoval, Dynamic modelling and control of MEA absorption processes for CO2 capture from power plants, Fuel, 116 (2014) 672-691.
[33] M. Panahi, S. Skogestad, Economically efficient operation of CO2 capturing process. Part II. Design of control layer, Chemical Engineering and Processing: Process Intensification, 52 (2012) 112-124.
[34] L. Faramarzi, E.S. Hamborg, S. Pedersen, B.F. Fostås, N.E. Flø, A.K. Morken, E. Gjernes, T.d. Cazenove, The third MEA Campaign at CO2 Technology Centre Mongstad, in, 4th Post Combustion CO2 Capture Conference PCC4 2017.
[35] M.R. Montañés, E.N. Flø, O.L. Nord, Dynamic Process Model Validation and Control of the Amine Plant at CO2 Technology Centre Mongstad, Energies, 10 (2017).
[36] E. Gjernes, S. Pedersen, T. Cents, G. Watson, B.F. Fostås, M.I. Shah, G. Lombardo, C. Desvignes, N.E. Flø, A.K. Morken, T. de Cazenove, L. Faramarzi, E.S. Hamborg, Results from 30 wt% MEA Performance Testing at the CO2 Technology Centre Mongstad, Energy Procedia, 114 (2017) 1146-1157.
[37] L. Faramarzi, D. Thimsen, S. Hume, A. Maxon, G. Watson, S. Pedersen, E. Gjernes, B.F. Fostås, G. Lombardo, T. Cents, A.K. Morken, M.I. Shah, T. de Cazenove, E.S. Hamborg, Results from MEA Testing at the CO2 Technology Centre Mongstad: Verification of Baseline Results in 2015, Energy Procedia, 114 (2017) 1128-1145.
[38] E.S. Hamborg, V. Smith, T. Cents, N. Brigman, O.F. Pedersen, T. De Cazenove, M. Chhaganlal, J.K. Feste, Ø. Ullestad, H. Ulvatn, O. Gorset, I. Askestad, L.K. Gram, B.F. Fostås, M.I. Shah, A. Maxson, D. Thimsen, Results from MEA testing at the CO2 Technology Centre Mongstad. Part II: Verification of baseline results, Energy Procedia, 63 (2014) 5994-6011.
[39] D. Thimsen, A. Maxson, V. Smith, T. Cents, O. Falk-Pedersen, O. Gorset, E.S. Hamborg, Results from MEA testing at the CO2 Technology Centre Mongstad. Part I: Post-Combustion CO2 capture testing methodology, Energy Procedia, 63 (2014) 5938-5958.
[40] E.M.B. Aske, S. Skogestad, Consistent Inventory Control, Industrial & Engineering Chemistry Research, 48 (2009) 10892-10902.
[41] R. Kehlhofer, B. Rukes, F. Hannemann, F. Stirnimann, Combined-Cycle Gas and Steam Turbine Power Plants (3rd Edition), in, PennWell, 2009.
[42] K. Jordal, P.A.M. Ystad, R. Anantharaman, A. Chikukwa, O. Bolland, Design-point and part-load considerations for natural gas combined cycle plants with post combustion capture, International Journal of Greenhouse Gas Control, 11 (2012) 271-282.
[43] F. Rezazadeh, W.F. Gale, K.J. Hughes, M. Pourkashanian, Performance viability of a natural gas fired combined cycle power plant integrated with post-combustion CO2 capture at part-load and temporary non-capture operations, International Journal of Greenhouse Gas Control, 39 (2015) 397-406.
[44] H.J. Christopher, K. James, How to determine a unit ramp rate (MW/min) for lowest total production cost, in, www.heatrate.com, 1987.

[45] S. Can Gülen, K. Kim, Gas Turbine Combined Cycle Dynamic Simulation: A Physics Based Simple Approach, Journal of Engineering for Gas Turbines and Power, 136 (2013) 011601-011601.
[46] M. Genrup, M. Thern, Ny gasturbinteknik 2012-2014: Gas Turbine Developments. Report 2012., in, ELFORSK, March 2013.
[47] J. Hentschel, U.a. Babić, H. Spliethoff, A parametric approach for the valuation of power plant flexibility options, Energy Reports, 2 (2016) 40-47.
[48] M. Panahi, S. Skogestad, Economically efficient operation of CO2 capturing process part I: Self-optimizing procedure for selecting the best controlled variables, Chemical Engineering and Processing: Process Intensification, 50 (2011) 247-253.
[49] S. Skogestad, C. Grimholt, The SIMC Method for Smooth PID Controller Tuning, in: R. Vilanova, A. Visioli (Eds.) PID Control in the Third Millennium: Lessons Learned and New Approaches, Springer London, London, 2012, pp. 147-175.
[50] S. Skogestad, I. Postlethwaite, Multivariable Feedback Control: Analysis and Design, John Wiley \& Sons, 2005.